INVESTIGATING RARE BIOMINERALIZATION STRUCTURES IN TRILOBITES

by

RAYA E GREENBERGER

ALBERTO PÉREZ-HUERTA, COMMITTEE CHAIR
C. FRED T. ANDRUS
KIMBERLY GENAREAU
SANDY EBERSOLE

A THESIS

Submitted in partial fulfillment of the requirements
for the degree of Master of Science
in the Department of Geological Sciences
in the Graduate School of
The University of Alabama

TUSCALOOSA, ALABAMA

2020

Copyright Raya E Greenberger 2020
ALL RIGHTS RESERVED

ABSTRACT

Trilobites, a diverse class of arthropods, inhabited a range of marine environments from Early Cambrian to Permian time, and their abundance and various morphologies are significant in the interpretation of evolution, paleoenvironments and biostratigraphy. Their preservation is due to their calcitic structures formed by biomineralization. Investigating biomineralization processes in trilobite can enhance our understanding of the evolution of trilobites. This thesis presents two rare biomineralization structures in trilobites; the *Asaphus* trilobites, displaying stalk eyes, varying in length and width, and the *Eldredgeops rana* trilobites, displaying patterns on their shells that may have served as an additional visual system or amorphous calcium carbonate reservoirs. The eyes of *Asaphus kowalewski, Asaphus cornutus and Asaphus punctatus* and the spots on the *Eldredgeops rana* were characterized using a scanning electron microscope for imaging, energy dispersive x-ray spectroscopy and electron backscattered diffraction mapping to obtain elemental composition and crystallographic orientation and to observe microstructural arrangements. Further analyses were done on the *Eldredgeops rana* trilobites using atomic force microscopy and Raman spectroscopy to study the surface of the spots and their chemical bonding, respectively. This study reveals the stalked eyes main features are lenses and fibers. *Asaphus kowalewski* has lenses shaped as a truncated prism. *Asaphus cornutus* and *Asaphus punctatus* have lenses that are shaped as either a cone or an elongated prism. The cone shaped lens resembles ommatidium in the compound eyes of modern arthropods. The variation in lens shape within a specie could be explained by sexual dimorphism, which has been reported in modern arthropods. These findings suggest a stronger evolutionary link between trilobites and

modern arthropods. Analysis of the spots on the *Eldredgeops rana* trilobite show that they cannot be lenses; there is no pathway connecting the spots to the exterior of the trilobite and no uniform orientation in the crystalline structures. Atomic force microscopy and Raman analyses of the spots show inconsistency with amorphous calcium carbonate. Overall, the results of this study demonstrate that by applying new concepts from the study of modern organisms and using advanced analytical techniques, we can enhance our understanding of the diversification of trilobites.

LIST OF ABBREVIATIONS AND SYMBOLS

AFM	Atomic force microscopy
EBSD	Electron backscatter diffraction
EDS	Energy dispersive x-ray spectroscopy
FE	Field emission
SE	Secondary electron
SEM	Scanning electron microscope
WD	Working distance
OIM	Orientation imaging microscopy
kV	Kiloelectron volt
µA	Microampere
E. rana	*Eldredgeops rana*
ACC	Amorphous calcium carbonate
cm	Centimeter
µm	Micrometers
$\bar{x}$	Mean
n	Sample size
Fe	Iron
Mg	Magnesium
Mn	Manganese
Sr	Strontium

P	Phosphorus
Na	Sodium
Ca	Calcium
S	Sulfur

ACKNOWLEDGEMENTS

I would first like to thank my committee chair, Dr. Alberto Pérez-Huerta, for his assistance with this project, including data collection, funding, and editing. I would also like to thank Dr. Fred Andrus, Dr. Kim Genareau, and Dr. Sandy Ebersole for serving as members of my thesis committee. I would like to thank Johnny Goodwin, Robert Holler and Rich Martens at the Central Analytical Facility for teaching me how to use the JEOL 7000 and TESCAN, and Michael Buettner of the Center for Materials for Information Technology for teaching me how to use the AFM. I would also like to thank Dr. Thomas A. Hegna, Anton Brodskiy and Markus Martin for providing these samples. I would like to acknowledge my sources of funding, including the University of Alabama Graduate School, The DGS Hook's Fund, and the University of Alabama Department of Geological Sciences. Finally, I would also like to thank my friends, especially the ones I made during my time at the Department of Geological Sciences, who have encouraged me and inspired me during my years at the University of Alabama and after, during the completion of my work. I would like to especially thank my mom for her continuous support of my education.

CONTENTS

LIST OF TABLES

LIST OF FIGURES

CHAPTER 1

INTRODUCTION

Biomineralization is the process by which organisms produce mineralized hard tissues. Biominerals are complex and hierarchical structures that fulfill a biological function, such as protection against predators, structural support, gravity sensors, reproduction and calcium storage for enhanced environmental adaptation and survival (Engel, 2017). Most biominerals are composites of two phases; a mineral phase(s) and an organic phase(s). The organic phase(s) are present inside the mineral (intra-crystalline) or in between crystals (inter-crystalline), forming an organic framework (e.g., collagen or chitin) for mineral growth and emplacement (Addadi et al., 2003; Weiner, 2008).

Calcium carbonate is the most abundant component of the mineral phase in terms of biomass and its ubiquitousness among mineralizing species (Lowenstam and Weiner, 1989). Among the eight known polymorphs of calcium carbonate calcite and aragonite are the dominant forms observed in nature.

The unique morphologies exhibited by biominerals cannot be synthesized abiotically. Studies have successfully formed some biominerals in the presence of specialized organically derived proteins (Evans, 2019). Biominerals often exhibit thermodynamically unstable or unlikely characteristics such as asymmetry not seen in inorganic mineral formation (Feng, 2011), demonstrating the strong genetic control that organisms possess over the biomineralization processes. Biological vital effects present challenges to the study of biominerals, as empirical

studies to quantify vital effects are often required for each individual species (Pérez-Huerta et al., 2018). Understanding the purpose and mechanisms that extant organisms use to exhibit biological control on the expression of the mineral phase and morphology of calcium carbonate in an evolutionary context may provide information about past environments that extinct organisms inhabited, as well as provide insight into the behavior and life-modes of those organisms (Weiner and Dove, 2003).

Trilobites, one of the earliest known classes of arthropods, are often well preserved in the fossil record due to their biomineralized exoskeletons and wide geographic distribution. They were abundant in numbers and taxa, and rich in morphological structures (Hughes, 2003). The frequent preservation of these structures gives scientists the unique opportunity to study and compare the numerous variations in morphology of the trilobite and provide insight to the evolution of the group, their life habits and the environment they inhabited.

Spiny limbs are indicative of predatory feeding and may have been used as jaws, picking and tearing up small prey (Fortey and Owens, 2003). Differences between thoracic and cephalic limbs suggest that the trilobite used some limbs to move and some limbs to process the sediment for food (Fryer, 1968). Thin-shelled trilobites were probably living in an oxygen-poor, but nutrient-rich environment, where they had no predators. (Fortey and Wilmot, 1991). Eye reduction or body shrinkage could be due to a long-term environmental change, such as a toxic environment or a mud blanket spread over a large area (Schoenemann, 2018).

Studying distinctive and rare structures in trilobites and the biomineralization mechanisms behind them can expand our understanding of evolution, geological events and biominerals.

Despite the difficulty synthesizing biominerals in the laboratory setting, many tools that are typically used to study inorganic minerals and manufactured materials can be utilized to study biominerals (Pérez-Huerta et al., 2018). For example, some biomineral structures consist of a mosaic of crystals and organic materials (Wilt, 1999), however, the structure acts as one single crystal optically and has near- identical x-ray diffraction properties (Simkiss, 1986). Atomic force microscopy (AFM), which provides information about mineral surface topography on the sub-nanometer scale, was used to characterize very subtle differences in crystal morphologies, as well as gather information regarding intra-crystalline organic matter (Cusak et al., 2008; Pérez-Huerta et al., 2013). Energy dispersive x-ray spectroscopy (EDS) and confocal Raman spectroscopy were used in the discovery and characterization of biominerals in acorn worms (Cameron and Bishop, 2012). Electron-backscatter diffraction (EBSD) can provide information regarding crystal orientation at the sub-microscopic scale, such as in the lenses of schizochroal trilobite eyes (Torney et al., 2014).

This study uses the techniques mentioned above to investigate two rare biomineral structures in trilobite. In the first case study, the eyes of *Asaphus cornutus, Asaphus punctatus and Asaphus kowalewski* are examined using SEM, EDS and EBSD. The purpose of these analyses is to observe internal structures, determine the type of lenses in the eye, compare between the species and evaluate the structural preservation. In the second case study, the spotted Eldredgeops rana is examined using SEM, EDS, EBSD, AFM and Raman. The purpose of these analyses is to compare to previous data and acquire additional information that may explain the presence of spots on the exoskeleton of the E. rana. The goal of this study is to advance our understanding of biomineralization structures and the processes by which they are created.

CHAPTER 2

CASE STUDY I: STALKED EYES IN *ASAPHUS* TRILOBITES

2.1 Introduction

The compound eyes of some arthropods taxa are one of the most common visual systems observed in the animal kingdom (Land and Fernald, 1992; Lee et al., 2012). The comparison of arthropod eye morphology in extant and extinct taxa can provide information about the development and evolution of the eyes, and the successful environmental adaptation of this group throughout the Phanerozoic. Trilobites, which were a highly diverse class of arthropods and abundant in Paleozoic seas, had compound eyes composed of biomineralized calcium carbonate (calcite) lenses. These lenses observed in trilobites represent one of the earliest and most sophisticated and complex visual systems among animals, as opposed to simpler systems of light-sensitive body part (Clarkson et al., 2006; Plachetzki et al., 2012).

There are three types of trilobite eyes observed in the trilobite fossil record: holochroal, schizochroal, and abathochroal. Holochroal eyes are found in specimens from as early as the lower Cambrian time period (Xi-Guang and Clarkson, 1990), and are the most common type found in trilobites (Fig. 1). Holochroal eyes are characterized by multiple small lenses, arranged in a close hexagonal packing (Clarkson et al., 2006). In contrast, schizochroal eyes, which are only found in the suborder Phacopina, have fewer and larger lenses, arranged in hexagonal packing but separated by sclera (Fig. 2) (Clarkson et al., 2006). Abathochroal eyes are only found in one suborder of small Cambrian trilobites, characterized by very small, separated lenses

(Clarkson et al., 2006).

According to Clarkson et al. (2006) and Miller and Clarkson (1980), schizochroal eyes consisted of a cornea underlain by an internal layered two lens structure (doublet) with different refractive indices to focus light. The layers consisted of lamellar calcite oriented such that its *c*-axis is parallel to the optic axis, and a lower bowl.

Holochroal eyes can be divided into two types: biconvex and prismatic planoconvex (Lindstörm, 1901, cited in Harrington, 1959). Biconvex lenses in holochroal eyes are thin lenses covered by a thin cornea; the lens' axial length is equal or smaller than the lens' diameter, and the internal and external shape of the lens is convex (Fig. 1D). Prismatic planoconvex lenses are characterized by hexagonal prisms covered by a thin cornea; the lenses have a longer axial length than diameter, and the external lens shape is planar (Fig. 1C).

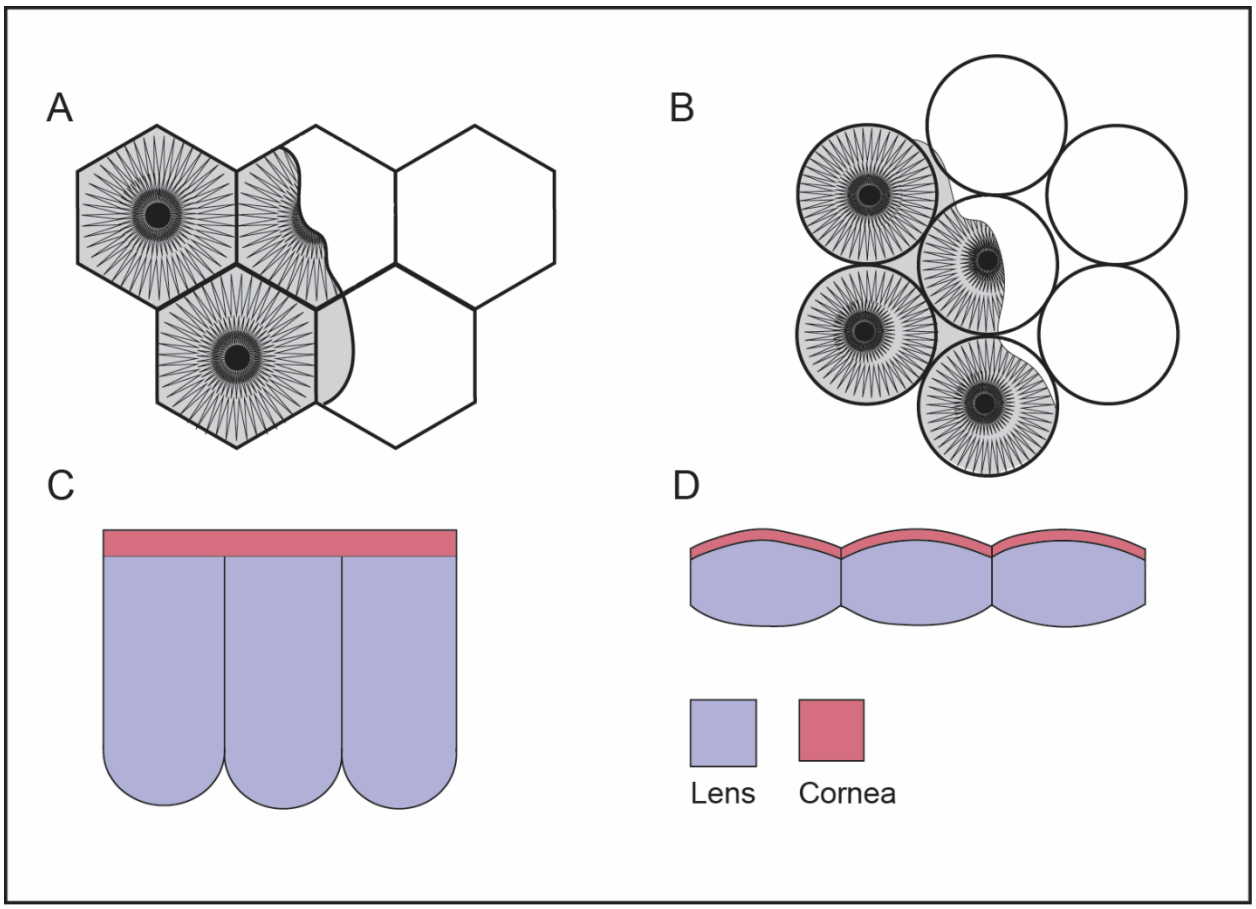

Figure 1. Illustrations of lens arrangement in holochroal eyes. A and B show hexagonal close packing. The calcite sheets (lamellae) below the cornea display radial arrangement. C and D cross section view. C is planoconvex, D is biconvex. Images are modified from Clarkson et al. (2006, figure 3).

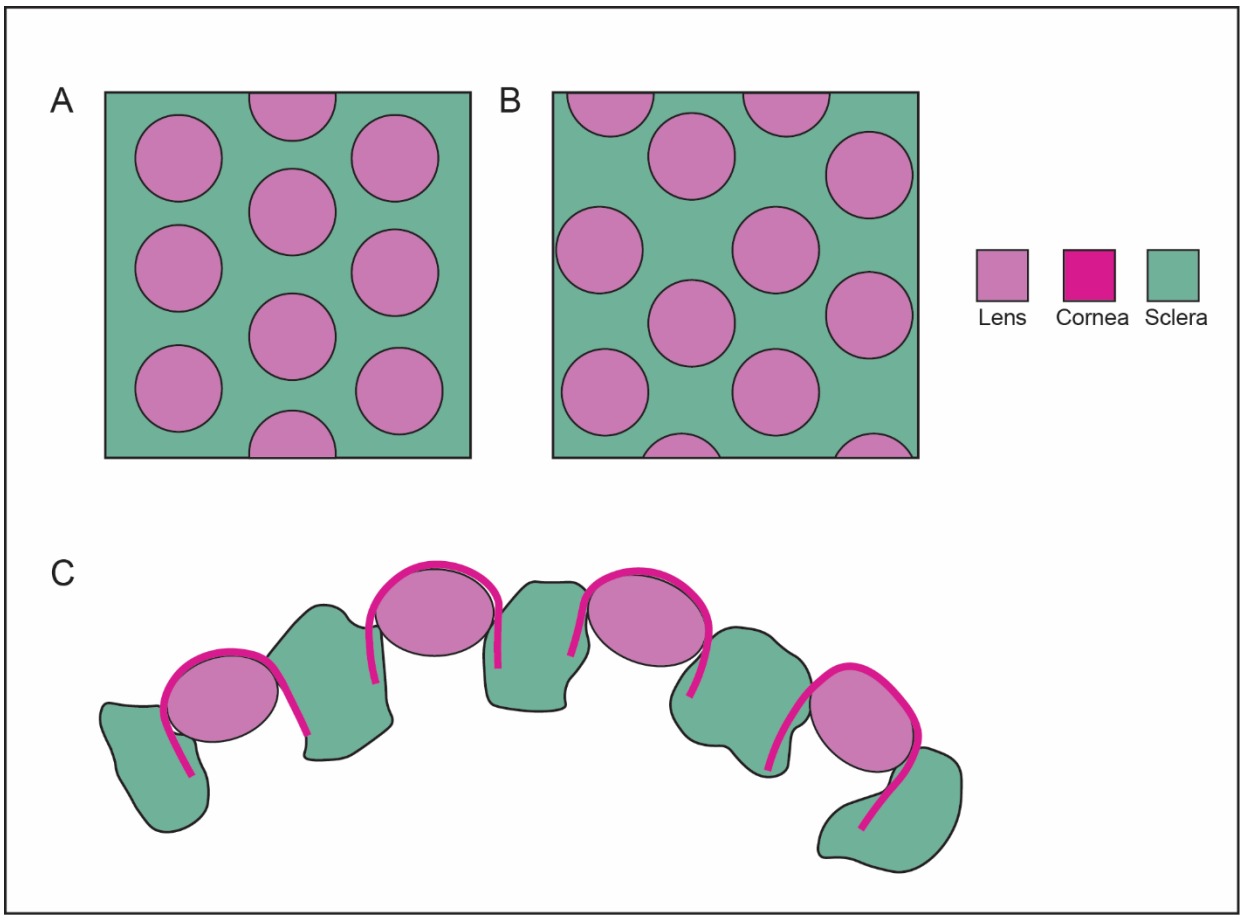

Figure 2. Illustrations of lens arrangement in Schizochroal eyes. A shows hexagonal packing. Each lens is surrounded by six equally spaced lenses. B shows cubic packing. Each lens is surrounded by four equally spaced lenses. C shows the cross section of *Geesops schlotheimi* eye. Images are modified from Torney (2010, figure 1.14).

Most trilobite species had a pair of compound eyes located on their cephalon (head section). Some species were blind or nearly blind and developed additional sensory organs (Whiteley et al., 2002). In contrast, species of the *Asaphidae, Encrinuridae*, and *Odontopleuridae* families developed elevated eyes, known as stalked eyes. A rigid stalked eye is also found in several insects, the most similar ones are the diopsinid flies (Peng et al., 2008; Warren and Smith, 2007).

Asaphus is a genus of trilobites that includes several species characterized by holochroal raised ("stalked") eyes (Fig. 3) which were first observed during the Upper Cambrian time period (Bell and Braddy, 2012). Dalingwater (1973) studied the eyes of *Asaphus raniceps* and determined that the eye in that trilobite species consisted of an external translucent layer (cornea) and an internal layer. The eyes had planoconvex lenses, where the internal layer consists of hexagonal calcite prisms with *c*-axes normal to the outer surface of the eye. According to Clarkson (1973), each prism in the *Asaphus raniceps* eye is a single crystal with a continuous, regular arrangement.

Fordyce and Cronin (1993) characterized the external holochroal eye structure of *Asaphus cornutus* from the Ordovician. They measured the azimuth and elevation of the lenses and noted there was a binocular overlap between the eyes; however, they did not study the internal structure. Based on observed similarities to the eyes of *Asaphus raniceps* (Clarkson, 1973), Fordyce and Cronin (1993) assumed the eyes of *Asaphus cornutus* were also made of hexagonal calcite prisms.

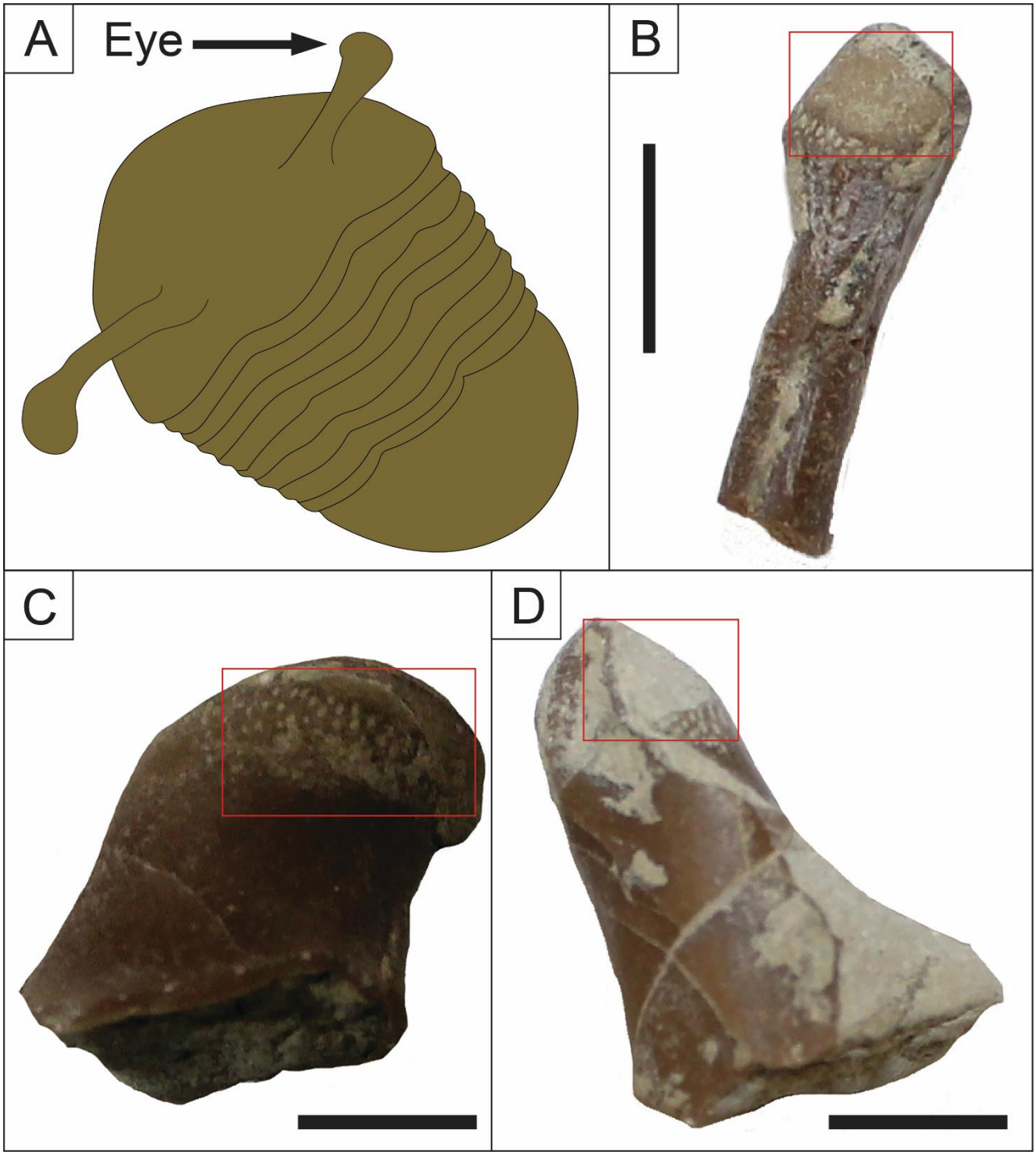

Figure 3. Illustration of a stalk trilobite and photos of one set of specimens. A. A generalized illustration of *Asaphus kowalewski* to demonstrate the location of the elevated eyes on the trilobite. Note the arrow to indicate the eye. B. *Asaphus kowalewski*. C. *Asaphus cornutus.* D. *Asaphus punctatus.* The red boxes in B-D outlines the lenses location on the eyes. Scale bar = 0.5 cm

2.2 Materials and Sample Preparation

2.2.1 Materials

Eyes of three species of Middle Ordovician *Asaphus* were collected near St. Petersburg, Russia and provided for this study by Dr. Thomas Hegna. The eyes included eight specimens of *Asaphus cornutus*, five specimens of *Asaphus punctatus*, and three specimens of *Asaphus kowalewski.* There are no visible lenses externally, however there are ridges in an area that may represent poorly preserved lenses (Fig. 3).

2.2.2 Sample Preparation

Three specimens of each specie were placed in epoxy resin and cut along their longest axis in the middle of the area of the lenses (Fig.3) to maximize the possibility of locating lenses. Grinding and polishing were done on Buehler abrasive paper and MicroCut discs (ranging from P280 to P2500) in three-minute intervals, and with a 1.0 and 0.3 micron MicroPolish at for 10 and 5 minutes, respectively. For SE imaging, samples were etched in 2% hydrochloric acid for 20 seconds and then gold coated for 1 minute using a sputter coater. For EDS and EBSD, samples were polished and coated with a 2.5 nm thick layer of carbon using a Gatan 681 coater.

2.2.3 Analytical Techniques

Secondary electron (SE) imaging was done on a JEOL 7000 field emission scanning electron microscope (FE-SEM) operated in high vacuum mode, at 30 kV, a medium beam current (6-13 µA) and 10 mm Working Distance (WD). EDS analysis was done with duplicate settings using Oxford Aztec EDS software. The microstructures of the eyes were characterized by electron backscatter diffraction (EBSD). EBSD maps were acquired in using JEOL 7000 FE-SEM in high vacuum mode, at 25 kV, a high beam current (14-18 µA) and 10 mm WD and approximately 0.5 step size. Further analysis of the EBSD maps was done using EDAX Orientation Imaging

Microscopy (OIM) software.

2.3 Results

SE images were conducted on nine specimens of stalked trilobite. The images revealed that all three species have the same three distinct structures and sections in the exoskeleton of the stalked eyes; lenses, granular non-structured features (non-lenses) and fibers. In situ, they all had a soft interior, now replaced by sand and large crystals (Fig. 4). All specimens of *Asaphus cornutus* and *Asaphus punctatus* display pristine lens structures consistently. One sample of *Asaphus kowalewski* displays undamaged lens structure, a second sample was partially damaged, and a third is extensively damaged (Fig. 7). The Asaphus species in this study display three different lens structures in four arrangements (Fig. 5). *Asaphus cornutus* and *Asaphus punctatus* lenses are either planoconvex with a cornea and a cone shaped lens, or planoconvex with a cornea and an elongated prism lens (Fig. 6). *Asaphus kowalewski* are planoconvex with a cornea and a truncated prism (Fig. 7).

All three species examined show fibrous structures adjacent to the lens section on both sides of the section (Fig. 8). All three species exhibit no structures in the non-lenses areas in the exoskeleton and show large crystals at the interior and exterior edges of the exoskeleton, and the inner-eye, sandy section. The crystal shape and locations are consistent between the three species (Fig. 9).

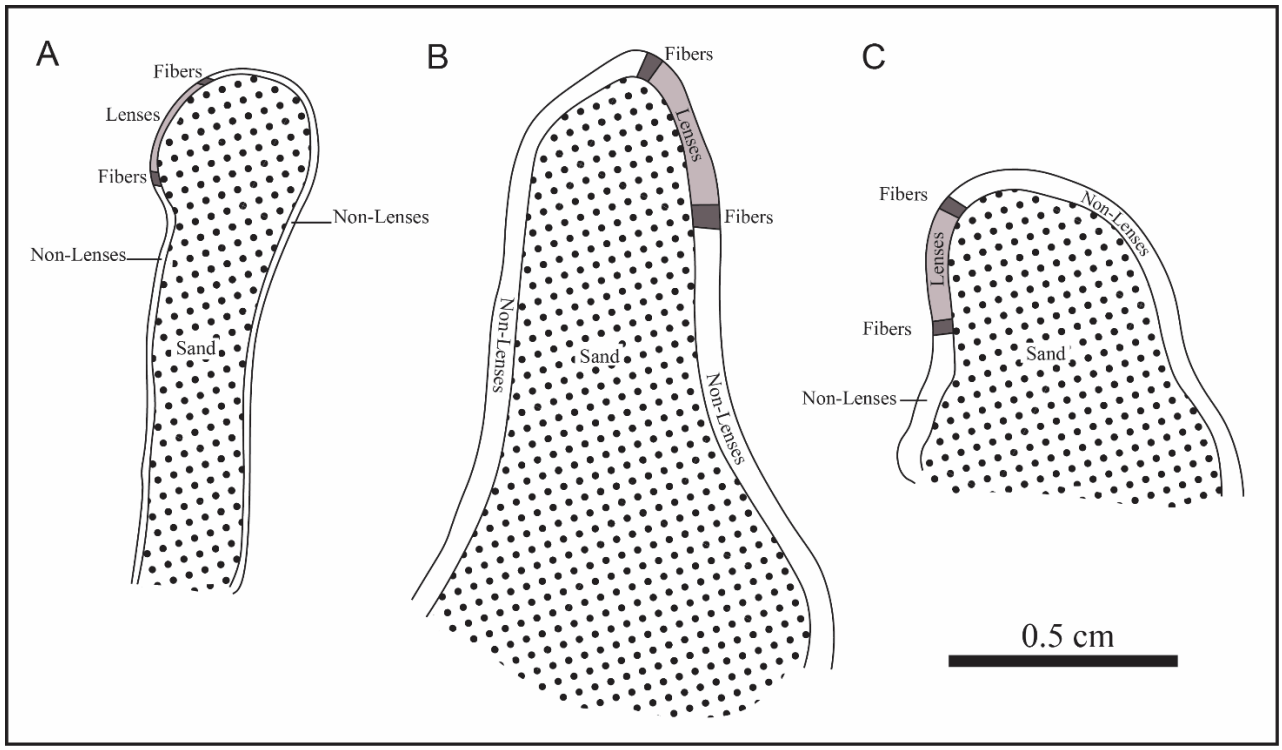

Figure 4. An illustration of the four different sections identified under SEM. A. *Asaphus cornutus* B. *Asaphus punctatus* and C. *Asaphus kowalewski*. All eyes have lenses, non-lenses, fibers, and an internal section composed of sand.

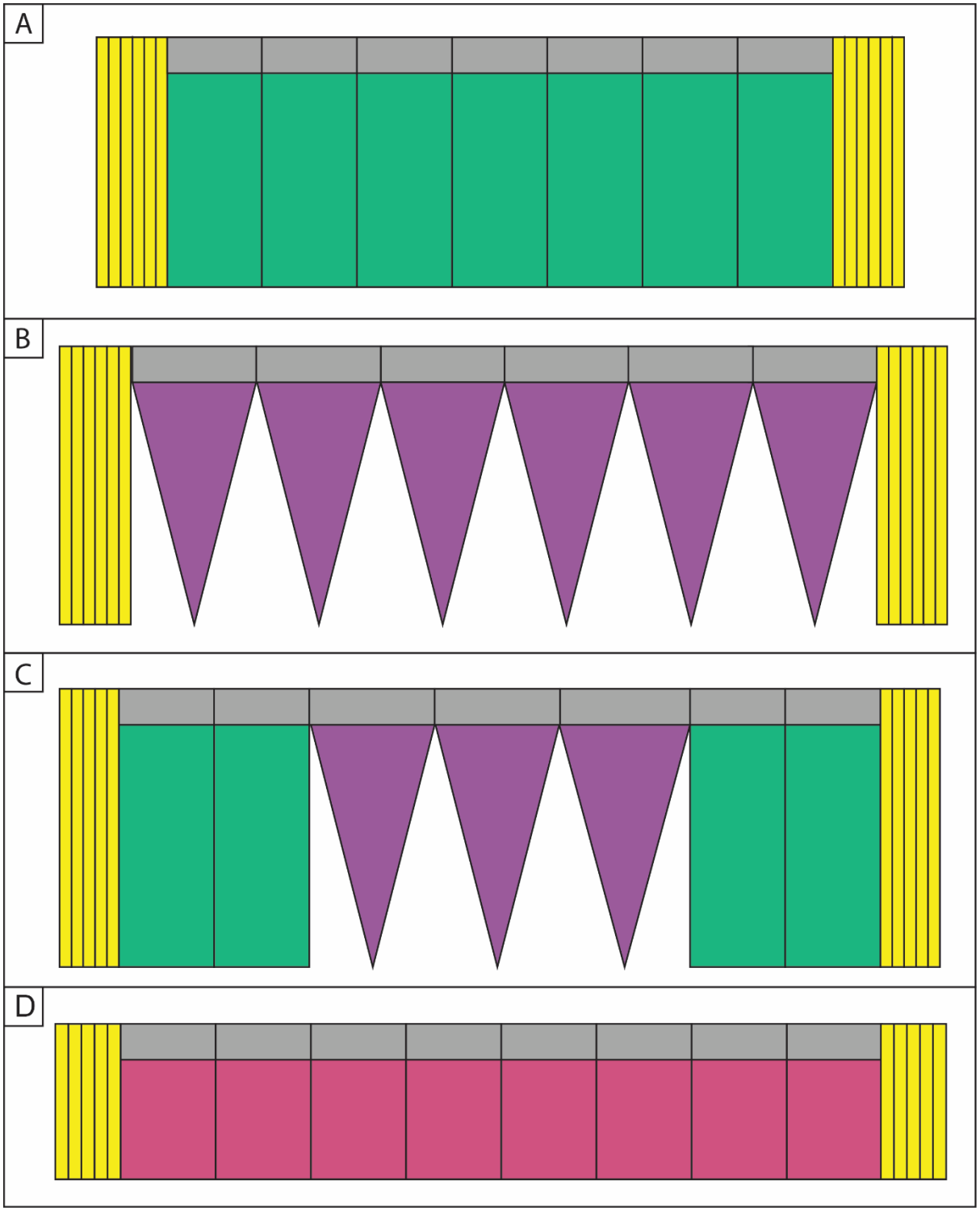

Figure 5. An illustration of four lens arrangements identified during secondary electron imaging. A. An all-elongated prisms structure. B. An all-cone crystal structure. C. A combined structure. D. A truncated prisms structure, seen only in *Asaphus kowalewski*.

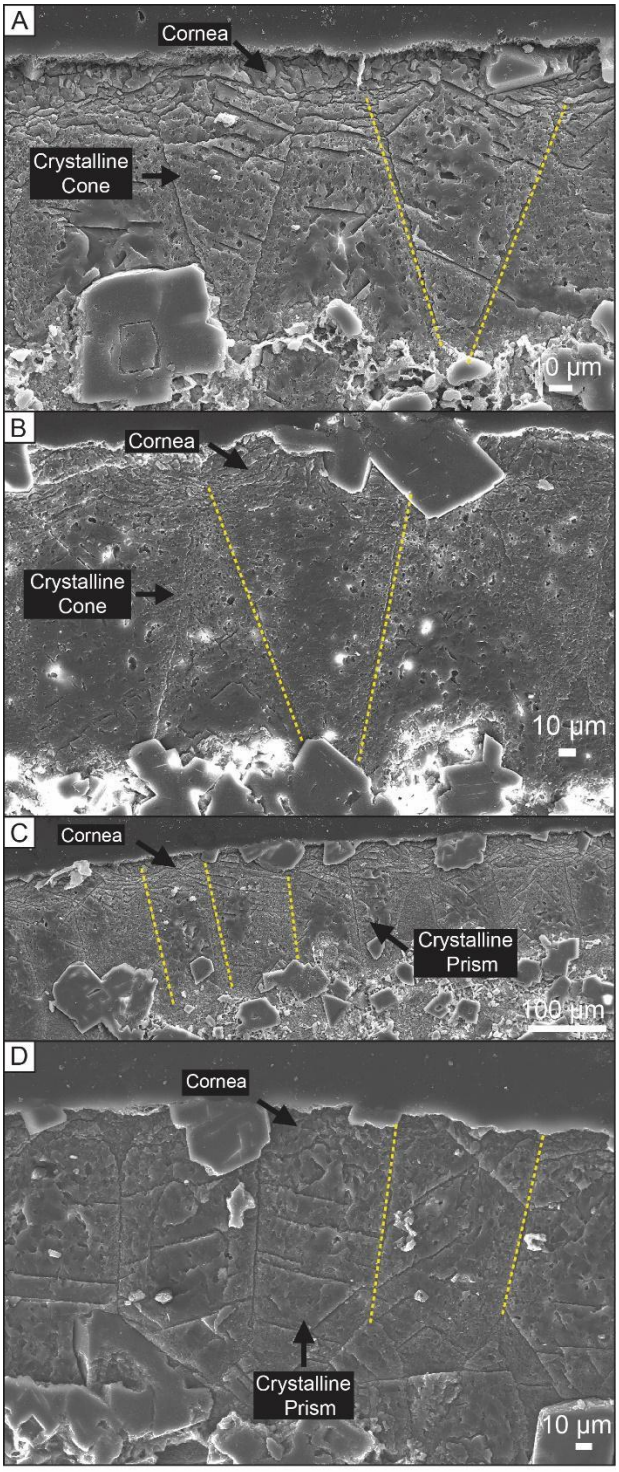

Figure 6. Secondary electron images comparing the lenses of stalked eyes trilobite. A. *Asaphus cornutus* showing a triangle shaped lens structure (yellow dash line). B. *Asaphus punctatus* showing a triangle shaped lens structure (yellow dash line). C. *Asaphus cornutus* showing an elongated prisms shaped lens structure (yellow dash line). D. *Asaphus punctatus* showing an elongated prisms shaped lens structure.

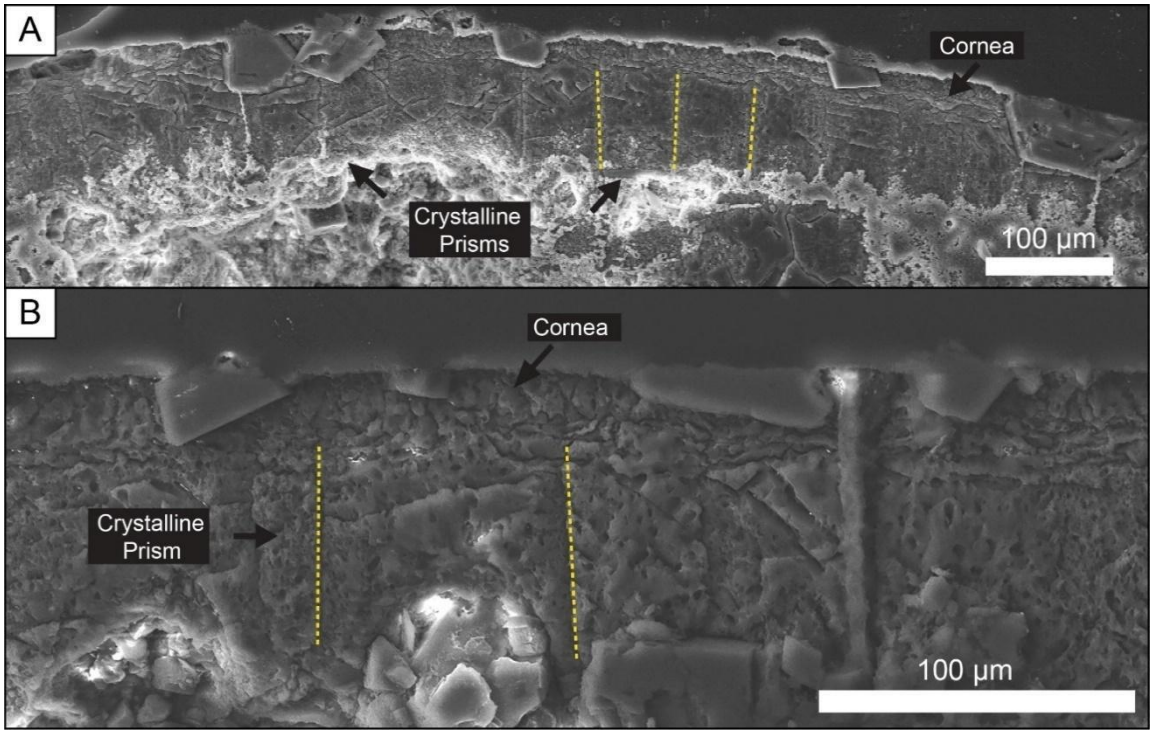

Figure 7. Secondary electron images of two *Asaphus kowalewski*. Both specimens show truncated prism shaped lens structure. Note the presence of patchy appearance of the lenses and the cavities below the lenses in A (indicated by the white areas).

The lenses of *Asaphus cornutus* are 70-190 µm in length ($\bar{x}$ =102 µm, n = 30 obtained from three specimens), 10-80 µm in width ($\bar{x}$ =53 µm, n = 30 obtained from three specimens) and have a 11-15 µm thick cornea ($\bar{x}$ =14 µm, n = 30 obtained from three specimens). The lenses of *Asaphus punctatus* are 130-218 µm in length ($\bar{x}$ =150 µm, n = 30 obtained from three specimens), 30-130 µm in width ($\bar{x}$ =86 µm, n = 30 obtained from three specimens) and have a 20-30 µm thick cornea ($\bar{x}$ =28 µm, n = 30 obtained from three specimens). The lenses of *Asaphus kowalewski* are 60-100 µm in length ($\bar{x}$ =86 µm, n = 20 obtained from two specimens), 31-60 µm in width ($\bar{x}$ =55 µm, n = 20 obtained from two specimens) and 11-23 µm thick cornea ($\bar{x}$ =20 µm, n = 20 obtained from two specimens).

In the *Asaphus cornutus*, the exoskeleton thickness in the fibrous region is 204-346 µm ($\bar{x}$

=285 µm, n = 12 obtained from three specimens). In the *Asaphus punctatus*, the exoskeleton thickness in the fibrous region is 224-446 µm ($\bar{x}$ =288 µm, n = 12 obtained from three specimens). In the *Asaphus kowalewski*, the exoskeleton thickness in the fibrous region is 149-197 µm ($\bar{x}$ =170 µm, n = 8 obtained from two specimens). In the *Asaphus cornutus*, the exoskeleton thickness is 347-447 µm ($\bar{x}$ =415 µm, n = 30 obtained from three specimens). In the *Asaphus punctatus*, the exoskeleton thickness is 585-673 µm ($\bar{x}$ =664 µm, n = 18 obtained from three specimens). In the *Asaphus kowalewski*, the exoskeleton is 251-358 µm thick ($\bar{x}$ =285 µm, n = 18 obtained from three specimens).

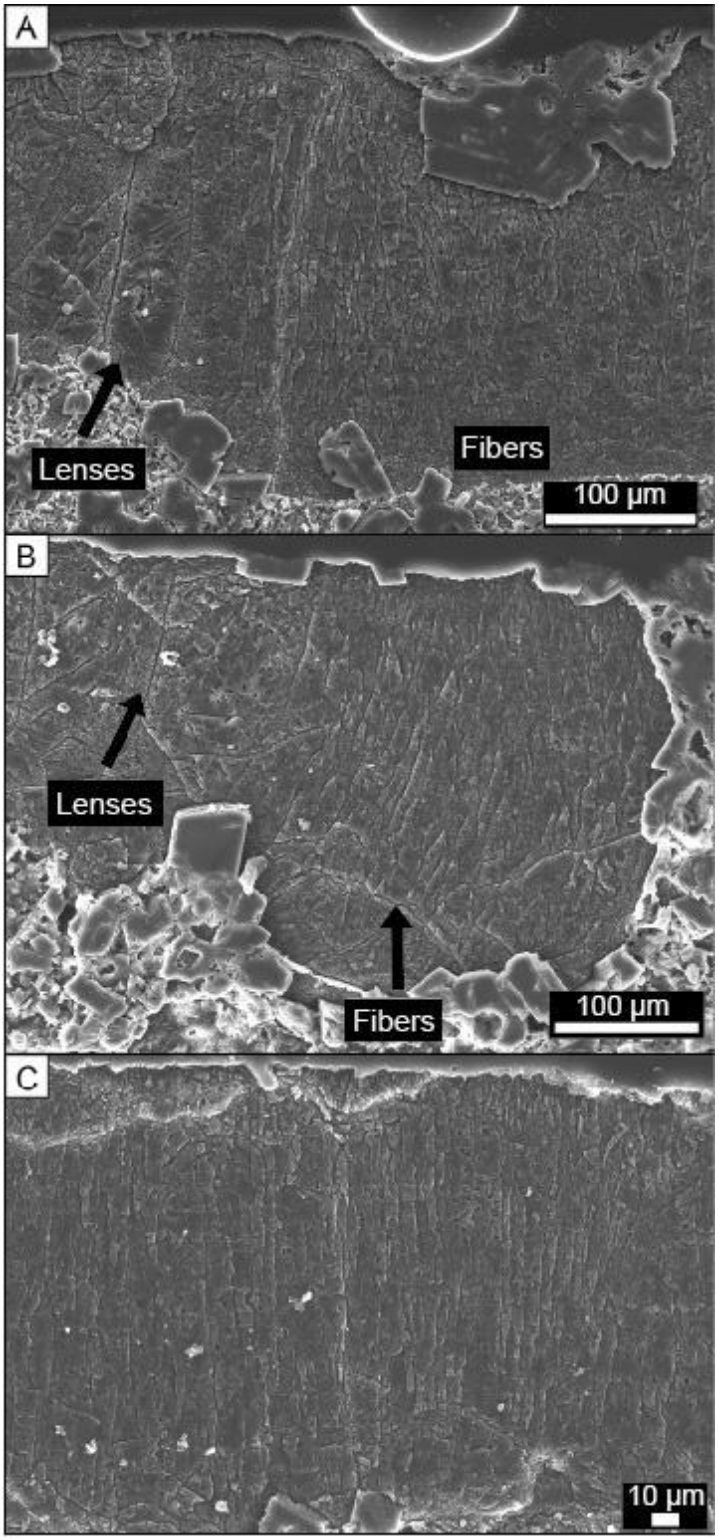

Figure 8. Secondary electron images of fiber-like structures adjacent to the lenses. A. *Asaphus cornutus.* B. *Asaphus punctatus.* C. *Asaphus kowalewski*. A and B show the boundary between fibers and lenses. C showing only fibers.

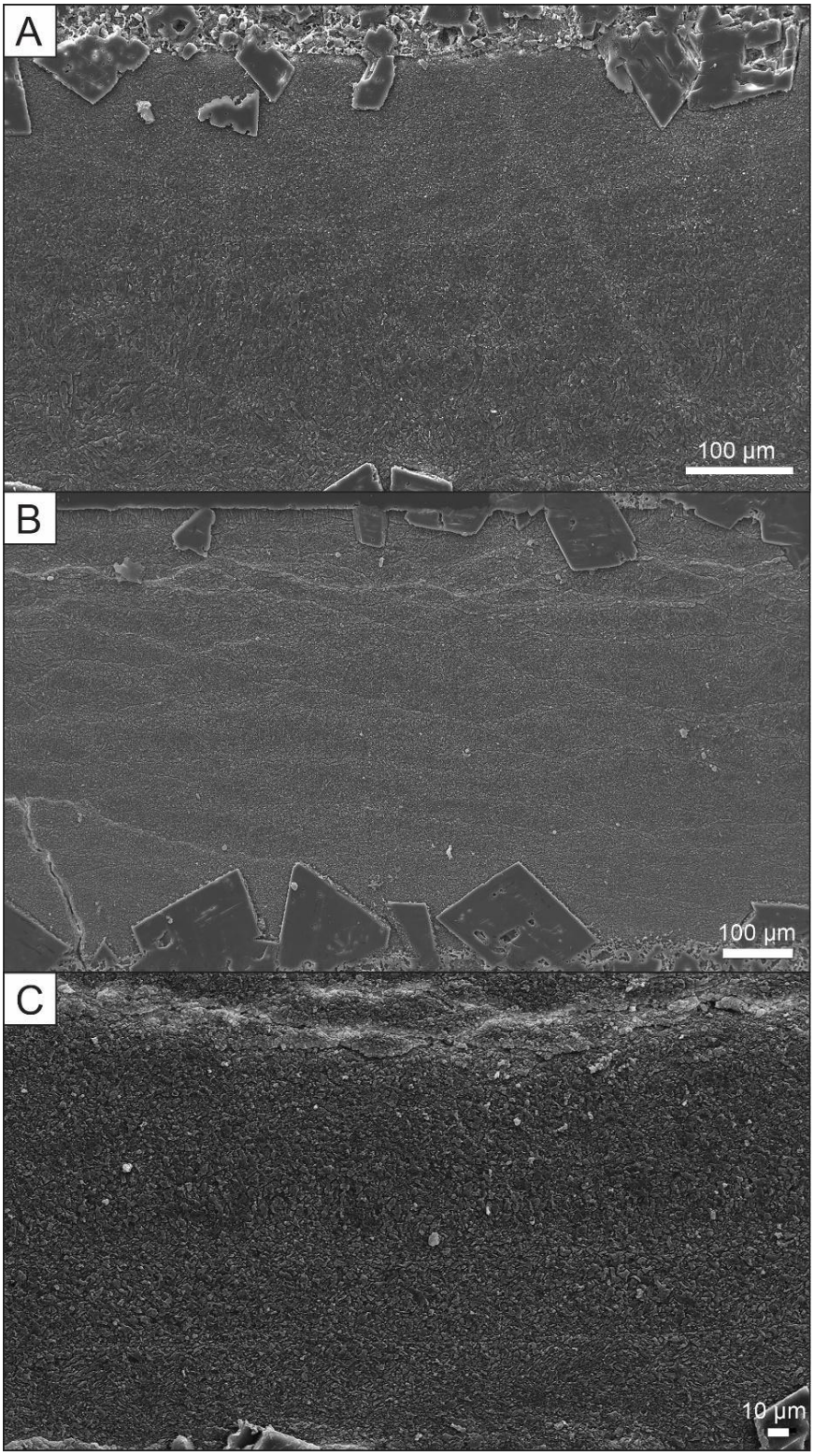

Figure 9. Secondary electron images of non-lenses sections in the stalk trilobite eyes. Note the lack of structures and presence of large crystals along the edges of the exoskeleton. A. *Asaphus cornutus.* B. *Asaphus punctatus,* and C. *Asaphus kowalewski*.

Elemental maps for the three species show many similarities. All of them show predominantly calcium, and lower concentrations of sodium, phosphorus, and sulfur in the lenses and cornea. The phosphorus and sulfur mirror each other, showing higher concentrations in the same areas (Fig. 10-12). The *Asaphus kowalewski* has the highest concentration of sulfur, compared to the *Asaphus cornutus* and the *Asaphus punctatus*. In all three species magnesium and strontium are concentrated in the large crystals at the edges of the exoskeleton.

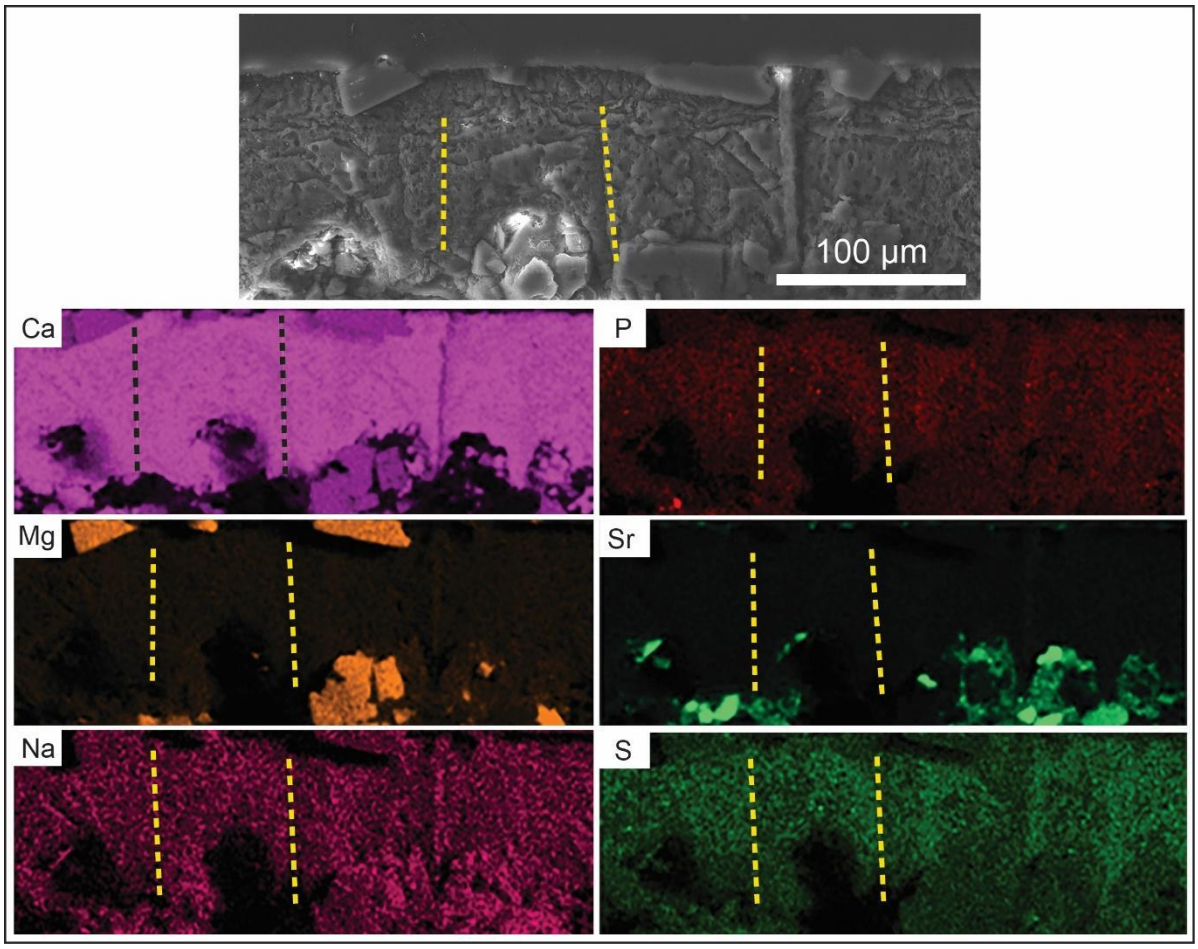

Figure 10. Energy dispersive x-ray spectroscopy maps of *Asaphus kowalewski*. The elements detected are noted in the top left box for each map. The yellow dash line outlines one of the lenses. Note the high concentration of Mg in the crystals above and below the lenses, and high concentration of Sr in the crystal below the lenses.

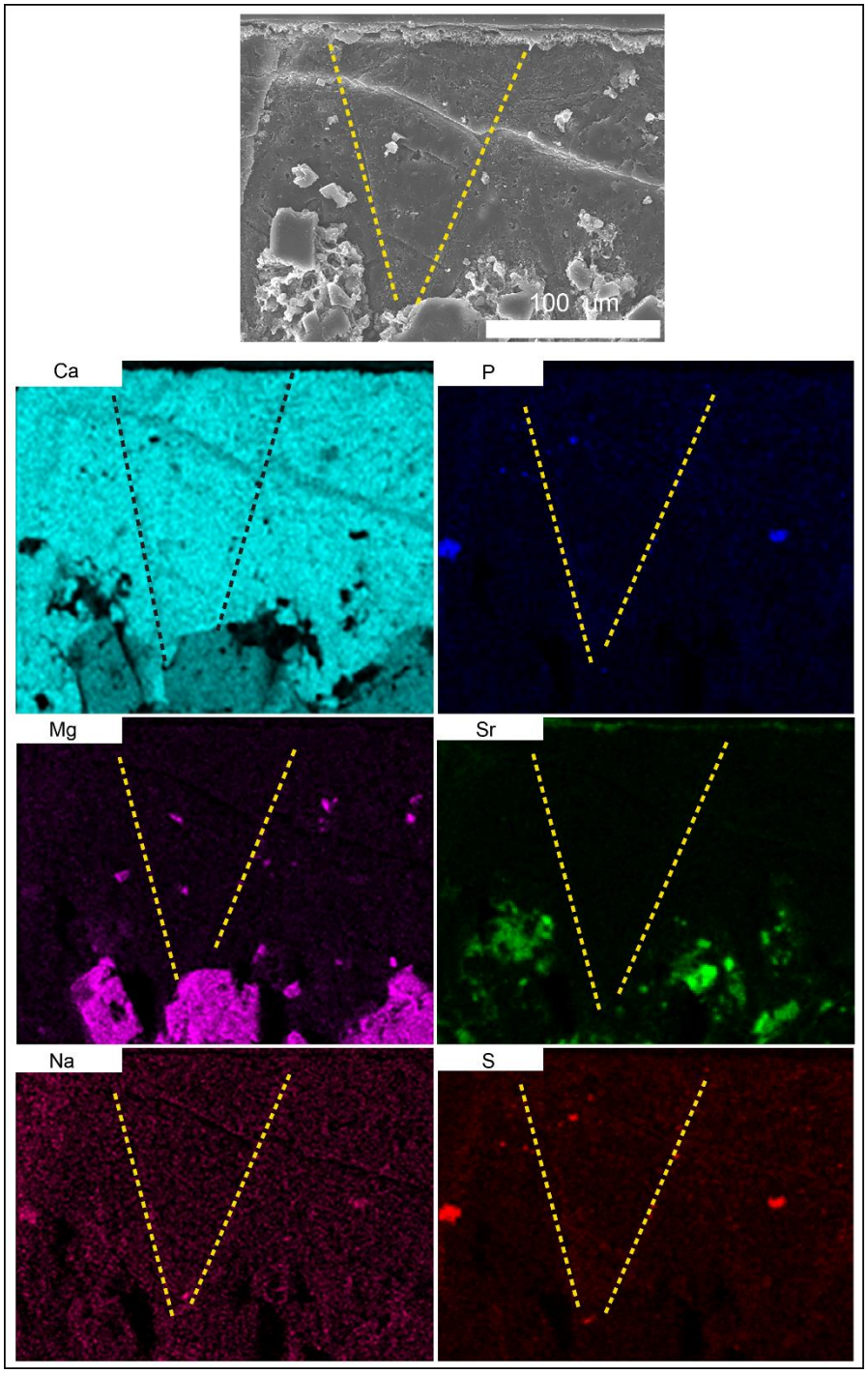

Figure 11. Energy dispersive x-ray spectroscopy maps of *Asaphus cornutus.* The elements detected are noted in the top left box for each map. The yellow dash line outlines one of the lenses. Note the high concentration of Mg and Sr in the crystal underlining the lenses.

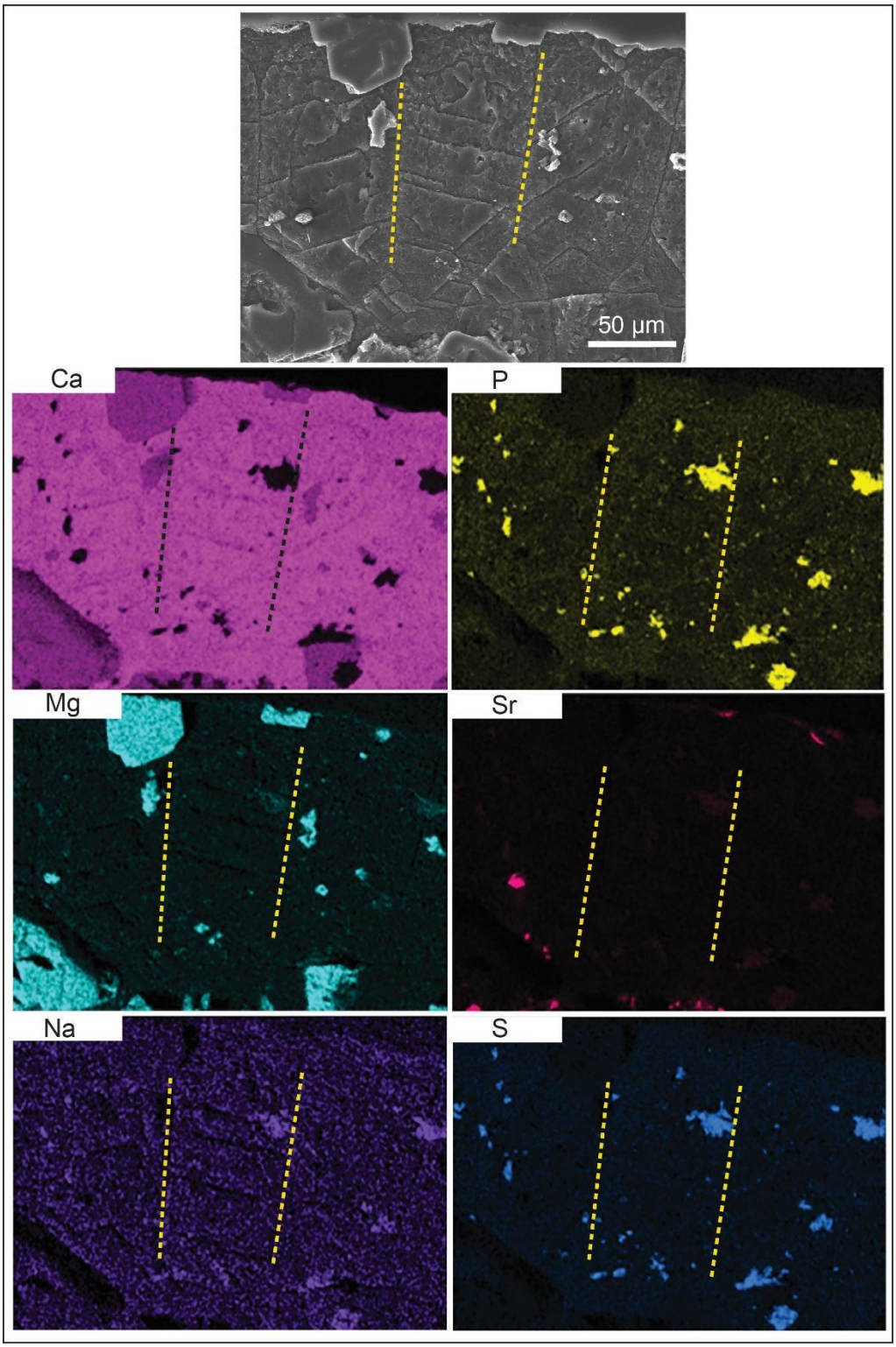

Figure 12. Energy dispersive x-ray spectroscopy maps of *Asaphus punctatus*. The elements detected are noted in the top left box for each map. The yellow dash line outlines one of the lenses. Note the high concentration of Mg in the crystals above and below the lenses.

EBSD mapping confirmed that the lenses are made of one crystal, in the shape of a prism or a cone, with similar orientation. The mapping also confirmed the arrangement of the lenses seen in SE images (Fig. 15B and 5). EBSD mapping revealed microcrystals in the corneas of *Asaphus cornutus* and *Asaphus punctatus* ranging from 5-15 µm. (Fig. 13B and 15B). These microcrystals were not visible in the cornea of *Asaphus kowalewski* (Fig. 17B).

EBSD mapping of the fibers revealed that individual fibers of *Asaphus kowalewski* are uniform in orientation, creating a lamellar structure (Fig. 18B). However, in *Asaphus cornutus* and *Asaphus punctatus*, the orientation of some of the fibers changes throughout the fibrous area (Fig. 14B and 16B).

Asaphus cornutus lenses display a similar c-axis orientation to the fibers but with a small range orientation; the pole figures of the lenses show a 30°- 60° range (Fig. 13C) whereas in the fibers the range is 20°- 60° (Fig. 14C). The pole figure of the *Asaphus punctatus* lenses show a constrained c-axis orientation around 45° (Fig. 15C). The c-axis orientation of the fibers has a variation of 45°-70° (Fig. 16C). *Asaphus kowalewski* lenses have a c-axis orientation of approximately 180° (Fig. 17C), while its fibers have orientation of approximately 180° and 360° (Fig. 18C). This degree of c-axis orientation means both lenses and the fibers are nearly perpendicular to the surface of the exoskeleton.

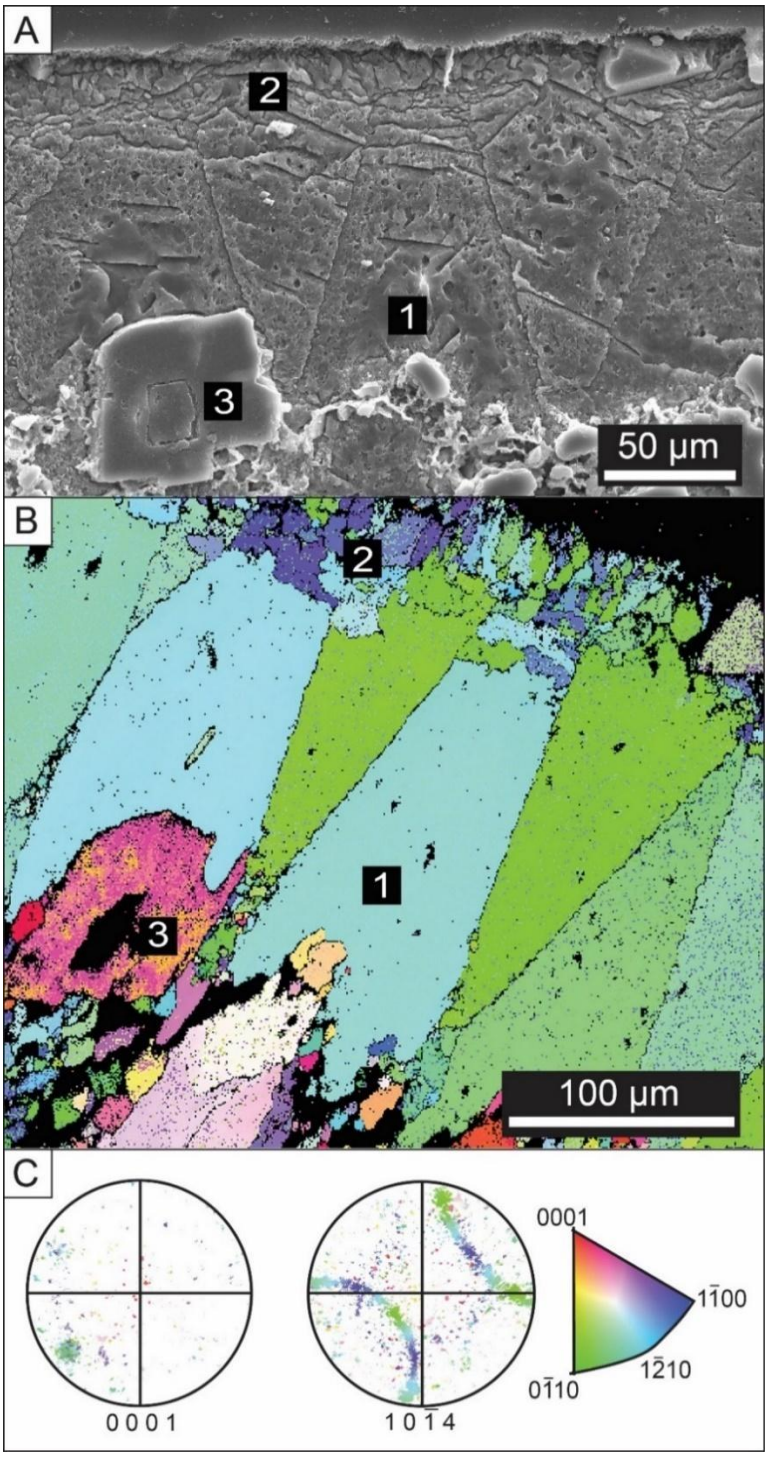

Figure 13. Lens crystal orientation in *Asaphus cornutus.* A. SE image of cone shaped lenses in *Asaphus cornutus*. B. A corresponding crystallographic map showing the microstructures of the corneas, and the crystal orientation of the lenses. The colors represent different planes of calcite as shown in the color key in C. C. Pole figures, corresponding to B, showing the crystallographic orientation of calcite crystals in reference to the {0001} plane and the {10$\underline{1}$4} plane.

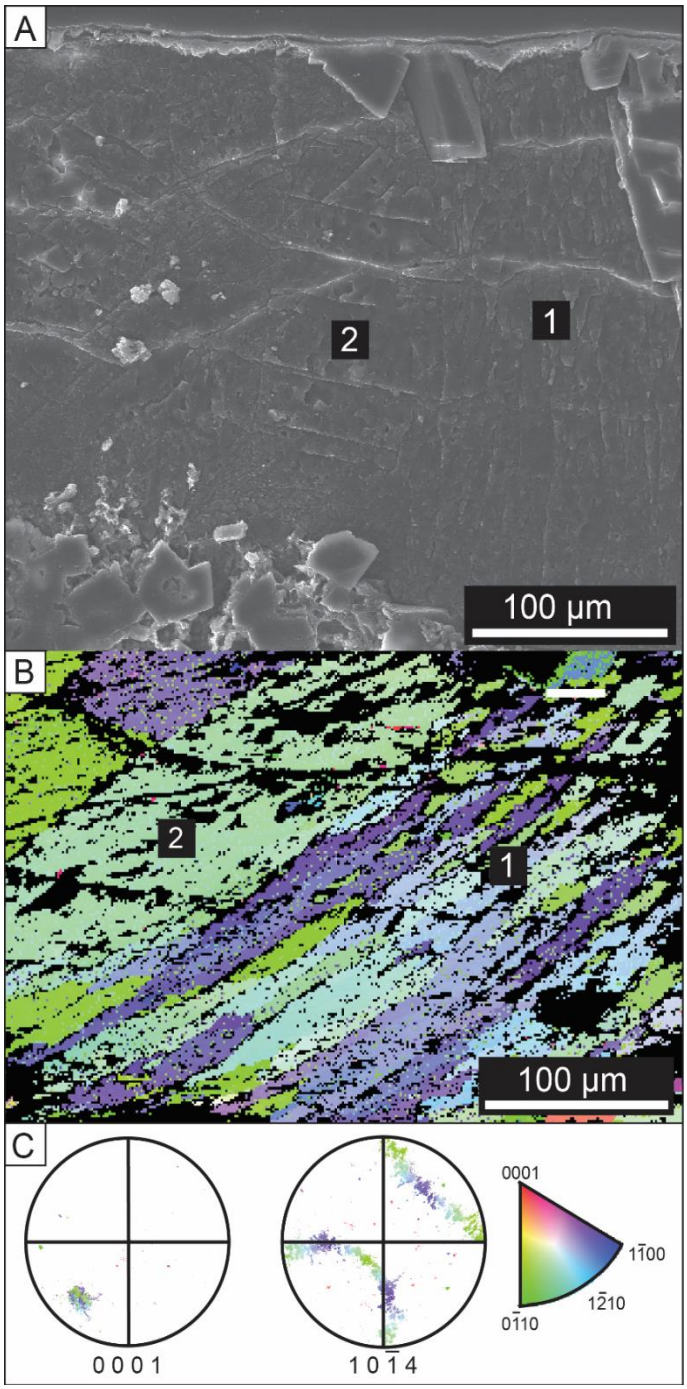

Figure 14. Fiber and lens crystal orientation in *Asaphus cornutus*. A. SE image of the boundary between the lenses and fiber structures. B. A corresponding crystallographic map showing the crystal structure and orientation of the lenses (2) and fibers (1). The colors represent different planes of calcite as shown in the color key in C. C. Pole figures, corresponding to B, showing the crystallographic orientation of calcite crystals in reference to the {0001} plane and the {10$\underline{1}$4} plane.

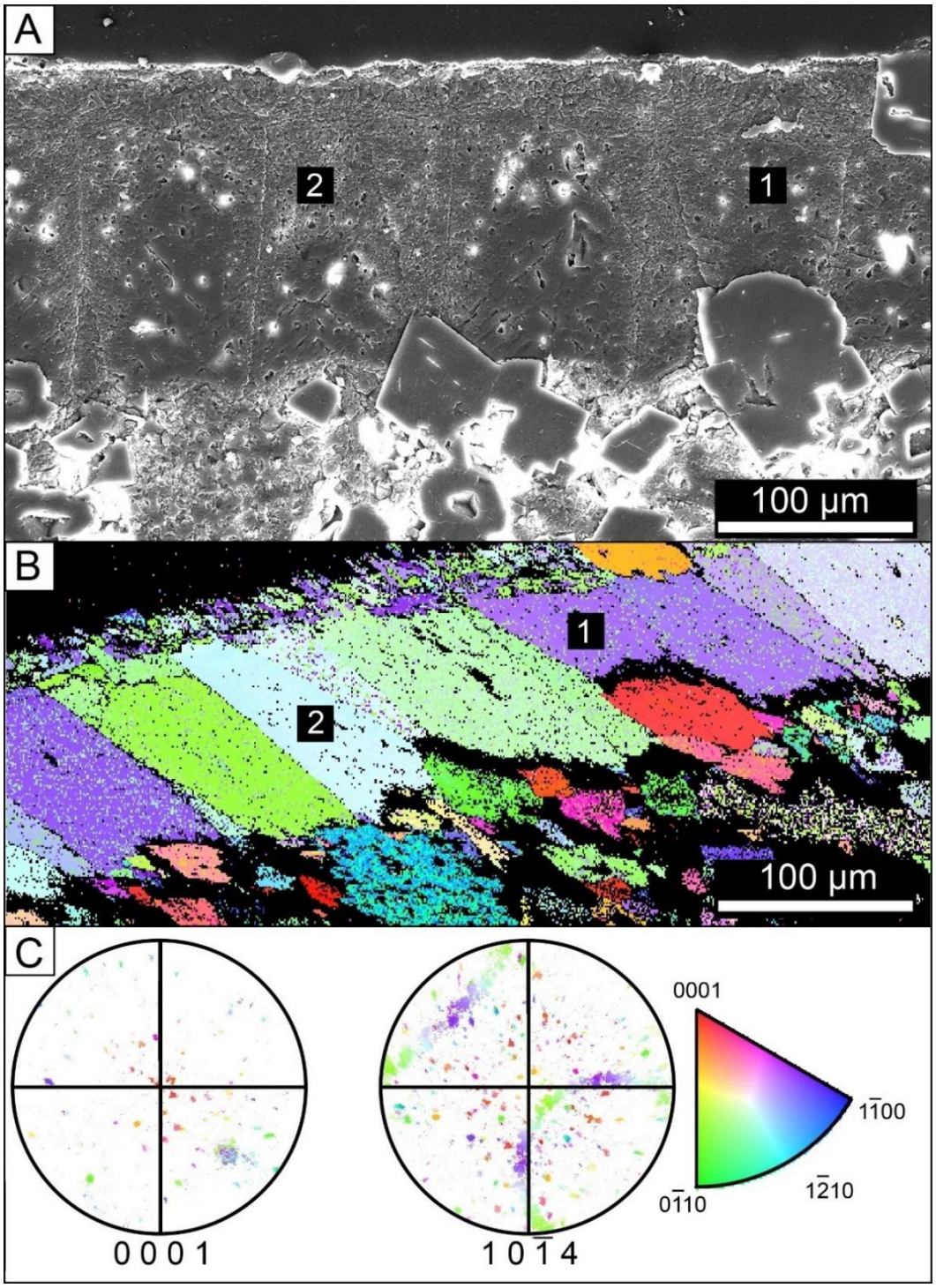

Figure 15. Lens crystal orientation in *Asaphus punctatus.* A. SE image of cone shaped and prism shaped lenses. B. A corresponding crystallographic map showing the microstructures of the corneas, and the crystal orientation of the lenses. The colors represent different planes of calcite as shown in the color key in C. C. Pole figures, corresponding to B, showing the crystallographic orientation of calcite crystals in reference to the {0001} plane and the {10$\underline{1}$4} plane.

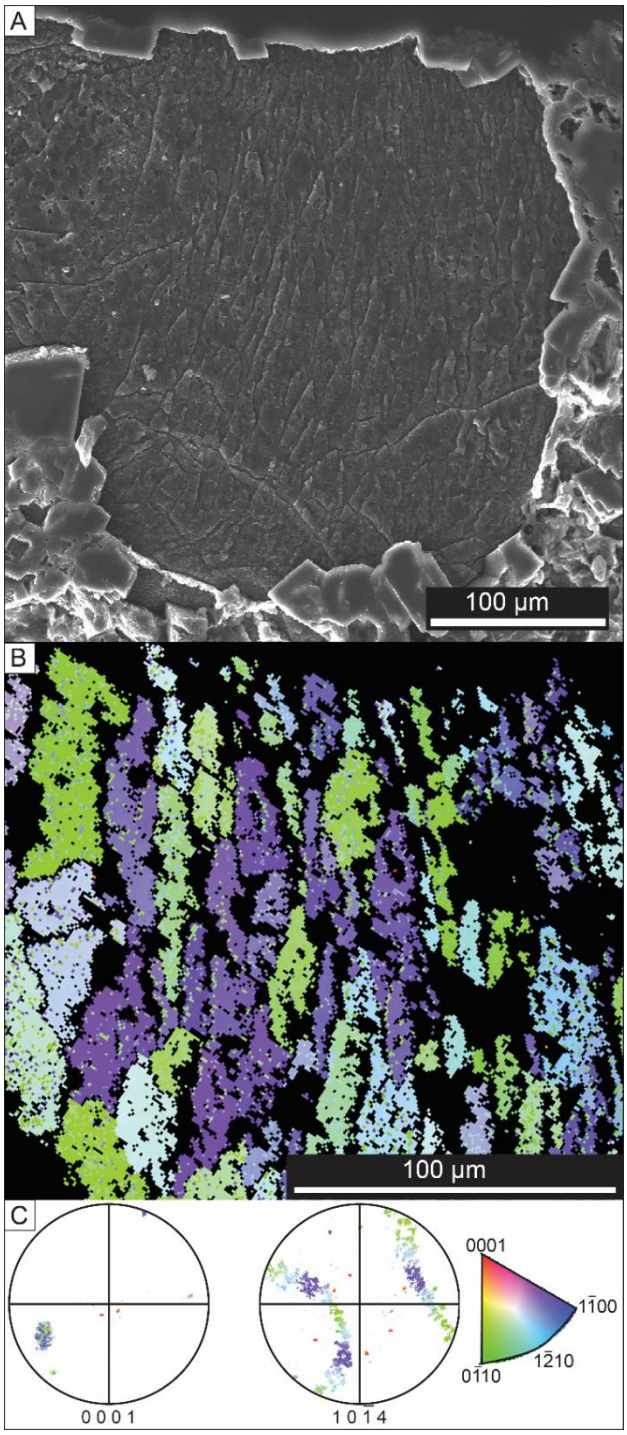

Figure 16. Fiber crystal orientation in *Asaphus punctatus.* A. SE image of fiber structures. B. A corresponding crystallographic map showing the crystal structure and orientation of fibers. The colors represent different planes of calcite as shown in the color key in C. C. Pole figures, corresponding to B, showing the crystallographic orientation of calcite crystals in reference to the {0001} plane and the {10$\underline{1}$4} plane.

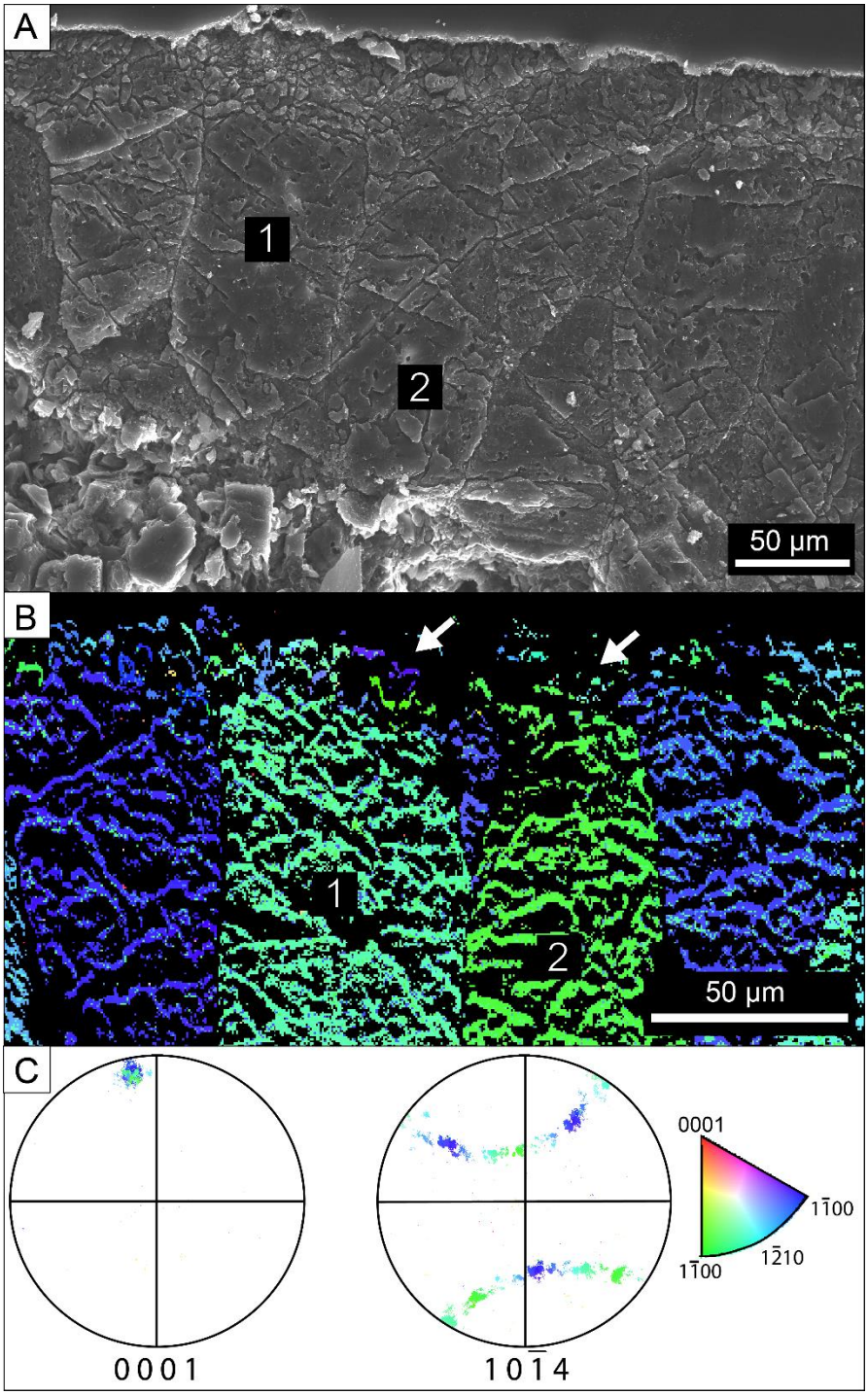

Figure 17. Lens crystal orientation in *Asaphus kowalewski.* A. SE image of prism shaped lenses. B. A corresponding crystallographic map showing the crystal structure and orientation of the lenses. Note the absence of crystallographic data in the corneas. The colors represent different planes of calcite as shown in the color key in C. C. Pole figures, corresponding to B, showing the crystallographic orientation of calcite crystals in reference to the {0001} plane and the {10$\underline{1}$4} plane.

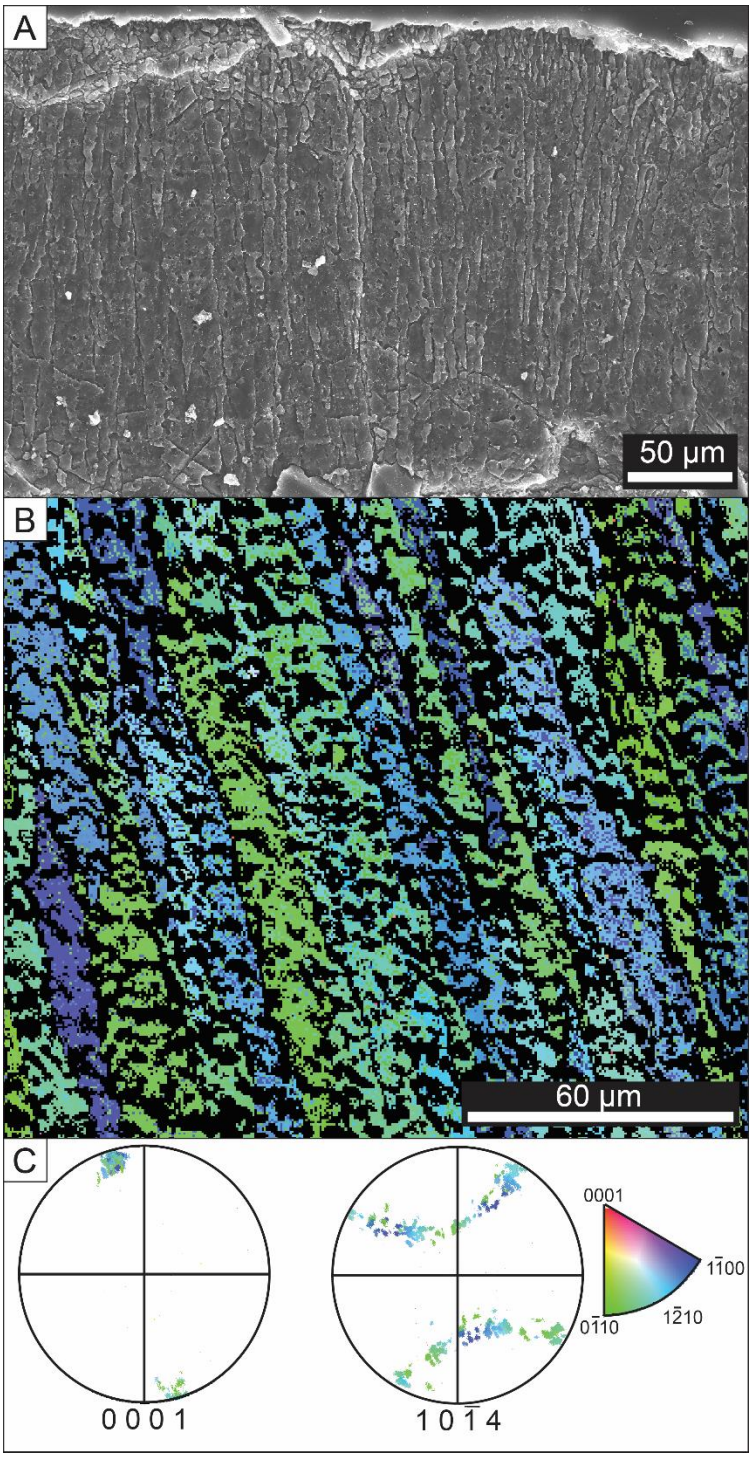

Figure 18. Fiber crystal orientation in *Asaphus kowalewski.* A. SE image of fiber structures. B. A corresponding crystallographic map showing the crystal structure and orientation of fibers. The colors represent different planes of calcite as shown in the color key in C. C. Pole figures, corresponding to B, showing the crystallographic orientation of calcite crystals in reference to the {0001} plane and the {10$\underline{1}$4} plane.

2.4 Discussion

A previous study of *Asaphus* trilobite lenses found that they are single prismatic crystal with two prismatic regions (Fig. 19) (Clarkson, 1973). This division is not evident in the lenses of *Asaphus cornutus*, *Asaphus punctatus*, and *Asaphus kowalewski*, but they do show a single prismatic crystal lens underlying a cornea. The three species have a planoconvex structure where the axial length of the lens is longer than the diameter, and the external lens shape is planar.

EBSD analysis showing individual crystals in the cornea (Fig. 13B and 15B) indicates recrystallization of the structure without altering its mineralogy. Microdolomite crystals seen in the exoskeleton boundaries are characteristic of replacement (Fig. 13B). Both forms of alteration are caused by an introduction of a fluid to the system (Lee et al., 2007). Despite diagenesis to the external and internal boundaries of the lenses, they are well preserved due to their heavy calcification and minimal organic material (McAllister and Brand, 1989).

Trilobite eyes are compound eyes. In an apposition compound eye, each ommatidium (single eye unit) receives light through the cornea and the lens and the image that is received is a composite of all the images. The sublensar section of the eye is organic and therefore is not preserved in trilobites. Modern low-light animals such as moths and mantis shrimps have similar external eye parameters to the *Asaphus cornutus* and so it has been suggested that they have similar ommatidium structure (Fordyce and Cronin, 1993). A similar study of the external measurements of the *Schimdtiellus reetae* Bergström, 1973 trilobite compound eye highlights their similarity to the eyes of bees and dragonflies and suggests the existence of a cone crystalline (Schoenemann et al., 2017).

The cone shaped lenses seen in the *Asaphus cornutus* and *Asaphus punctatus* in this study

are similar to the crystalline cones seen in apposition compound eyes in modern crustaceans and insects (Fig. 20), strengthening the hypothesis that trilobite eyes operated the same way as modern arthropod. The compound eyes of crustaceans and insects are composed of optic units (ommatidium). The eye forms a mosaic image that would allow them to detect obstacles and other organisms. The cone shaped lenses of the *Asaphus cornutus* and the external eye parameter measurements done by Fordyce and Cronin (1993) also strengthen the hypothesis that the eyes were likely used in low-to-moderate light environments.

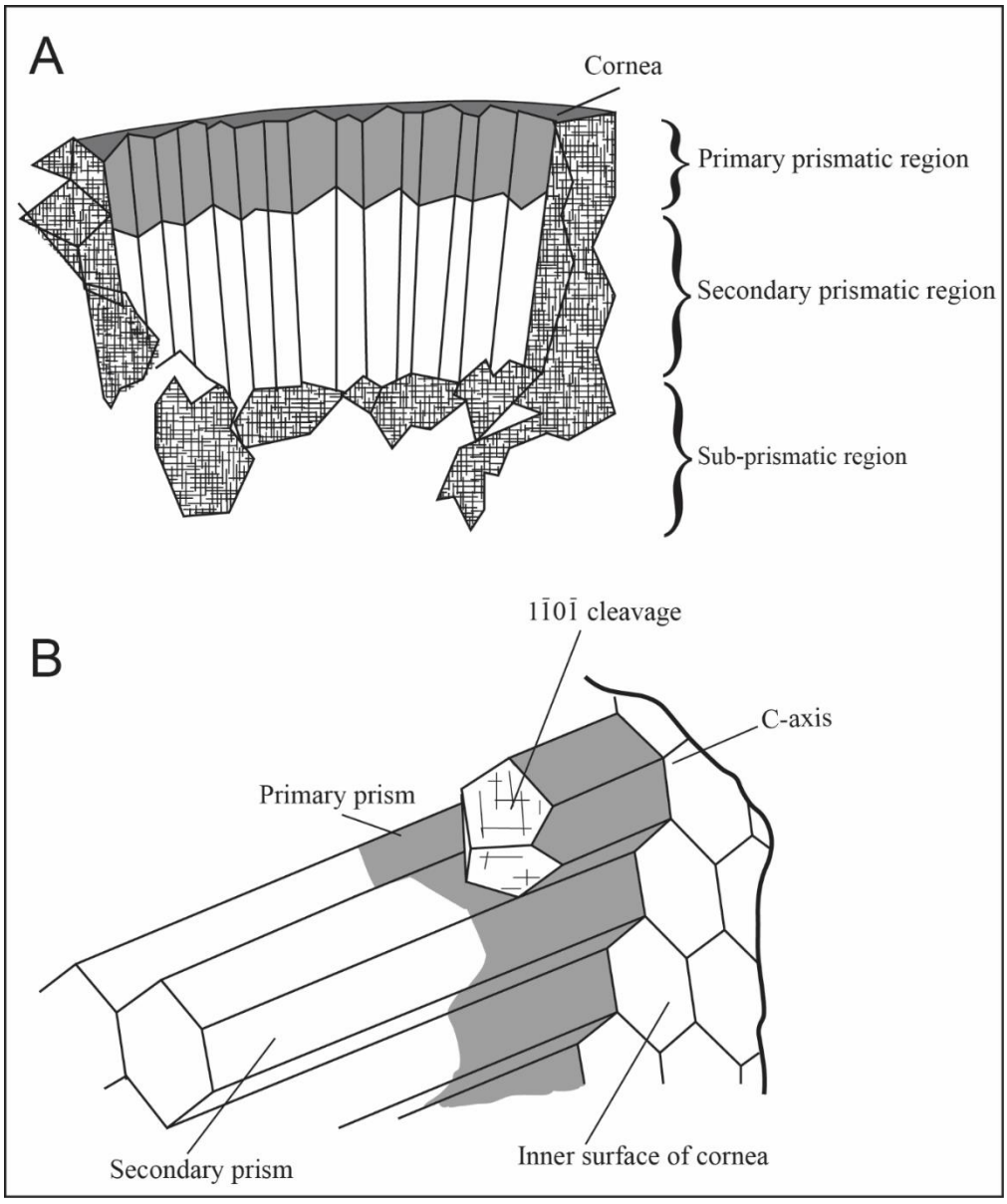

Figure 19. Illustrations of visual structures observed in *Asaphus* raniceps. A. Shows the division of the eye to four regions. Note the division to two prismatic regions. B. Shows the normal orientation of the lenses (prisms) relative to the inner surface of the cornea and the external surface of the eye. Images are modified from Clarkson (1973, figure 1).

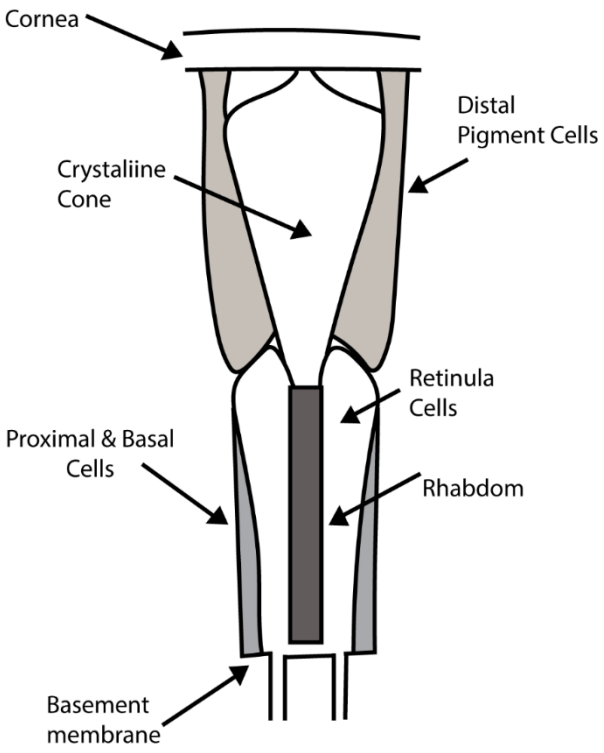

Figure 20. An illustration of a single ommatidium of a crustacean opposition compound eye. Note the crystalline cone underlying a cornea. Image is modified from Fordyce and Cronin (1993, figure 1).

Sexual dimorphism could explain the variation of lens shape (prism and cone) in *Asaphus cornutus*, and *Asaphus punctatus* (Fig. 5). It can be found in modern arthropods, such as the stalk-eyed fly. The male fly has a larger eye span because his ability to attract females by maintaining mating sites is affected by the size of his eye span (Baker and Wilkinson, 2001). In the *Acentria ephemerella*, a low light moth, the ommatidium of the male eye has longer dioptric crystalline cones and light-perceiving elements, which gives him superior visual sensitivity in dim conditions and the ability to detect movement during the day (Lau et al., 2008). In *Heliconius erato*, nymphalid butterfly, females express the two UV opsin proteins (UVRh1 and UVRh2) in separate photoreceptors, but males only express UVRh2. This may be due to the females' need to differentiate between conspecifics and co-mimics (McCulloch, Osorio, and

Briscoe, 2016).

EBSD data reveals that the fibers and the lenses have similar c-axis orientation implying the fibers serve an optical function. For the *Asaphus cornutus, Asaphus punctatus*, and *Asaphus kowalewski*, the location and properties of the fibers may be an indication that the lens grew and mineralized from lamella, retaining some layers as reserve for lens crystallization during molting or as a protective layer (Schoenemann, 2018; Miller and Clarkson, 1980).

2.5 Conclusions

The *Asaphus cornutus*, *Asaphus punctatus* and *Asaphus kowalewski* eyes were analyzed for their structure, chemical composition, and crystallographic orientation. Four sections were seen in all three species: lenses, non-lenses, and fibers in the exoskeleton, and an internal section composed of sand and microdolomite crystals. The thin stalked eye of *Asaphus kowalewski*, displayed poorly preserved planoconvex lenses with a truncated prism. The thick stalked eyes of *Asaphus cornutus* and *Asaphus punctatus* displayed better preserved planoconvex lenses with an elongated prism lens or a cone shaped lens. The cone shaped lenses seen in the *Asaphus cornutus* and *Asaphus punctatus* are similar to the crystalline cones seen in apposition compound eyes in modern crustaceans and insects. This finding provides another clue to the phylogenetic position of trilobites within the arthropods, suggesting they are closer to crustaceans and insects. It also suggests that they were able to see low-resolution images. EBSD data revealed that both the lenses and the fibers are nearly perpendicular to the surface of the exoskeleton, indicating that the fibers serve an optical function. This finding provides insights to the biomineralization processes that form the calcitic lenses. The variation of lens shape (prism and cone) in *Asaphus cornutus* and *Asaphus punctatus* could be explained by sexual dimorphism, which is seen in modern day stalked eyes of insects. The finding suggests a more direct phylogenetic link to

insects. The data also show microdolomite crystals in the exoskeleton boundaries, characteristic of replacement due to an introduction of a fluid to the system. Despite the diagenesis, original structures are preserved in the lenses due to their calcitic composition.

CHAPTER 3

CASE STUDY II: SPOTTED *ELDREDGEOPS RANA* TRILOBITE

3.1 Introduction

Color markings are rarely preserved in the fossil record, but they are typically found on the exoskeleton. These markings can result from biological or a structural process: biochromes, which are pigments formed by epidermal cells, or sclerochromes, which are structural colors, and appear as iridescence on shells. (Fox, 1972). These markings may provide information regarding the habitual relationships of the trilobite and may indicate a need for camouflage (Kobluk and Mapes, 1989; Hollingworth and Barker, 1991). Additionally, observed colors do not always represent the original colors because the exoskeleton may have gone through diagenetic mineralization. (McRoberts et al., 2013).

The Eldredgeops rana trilobites were collected from the Middle Devonian Hamilton Group in central and western New York by McRoberts et al. (2013). The trilobites were found in a gray carbonate mudstone with some pyrite replacement present. The specimens display pigmented spots on the dorsal surface of their exoskeleton (Fig. 21). Some specimens have a light-colored exoskeleton with dark spots (Fig. 21A and 21B), while others have a dark-colored exoskeleton with light spots (Fig. 21C). Some spots appear isolated while some appear fused together. McRoberts et al. (2013) examined the spots and found that they are embedded in the exoskeleton. They also determined that the exoskeleton and the spots have the same composition of low-Mg

microcrystalline calcite with trace amounts of Sr, Mn, Fe, and Na.

The role of the spots is not clear, and in this study I examined two possibilities:

1. The spots are lenses, serving a similar function to mineral lenses used in light detection found in modern brittle stars. Brittle stars have lenses composed of calcite crystal that focus light into the organisms' nerve system (Aizenberg et al., 2001). Chitons have hundreds of microscopic aragonite lenses on their shells (Li et al., 2015).

2. The spots are micron-sized spheres of preserved stable amorphous calcium carbonate (ACC). All arthropods, including trilobites, periodically shed the exoskeleton to grow. ACC has been linked to the process of molting in some modern arthropods (Dillaman et al., 2005). ACC is unstable in its pure form, but it can be stable as a biomineral in the presence of phosphate and in an anhydrous state (Albéric et al., 2018).

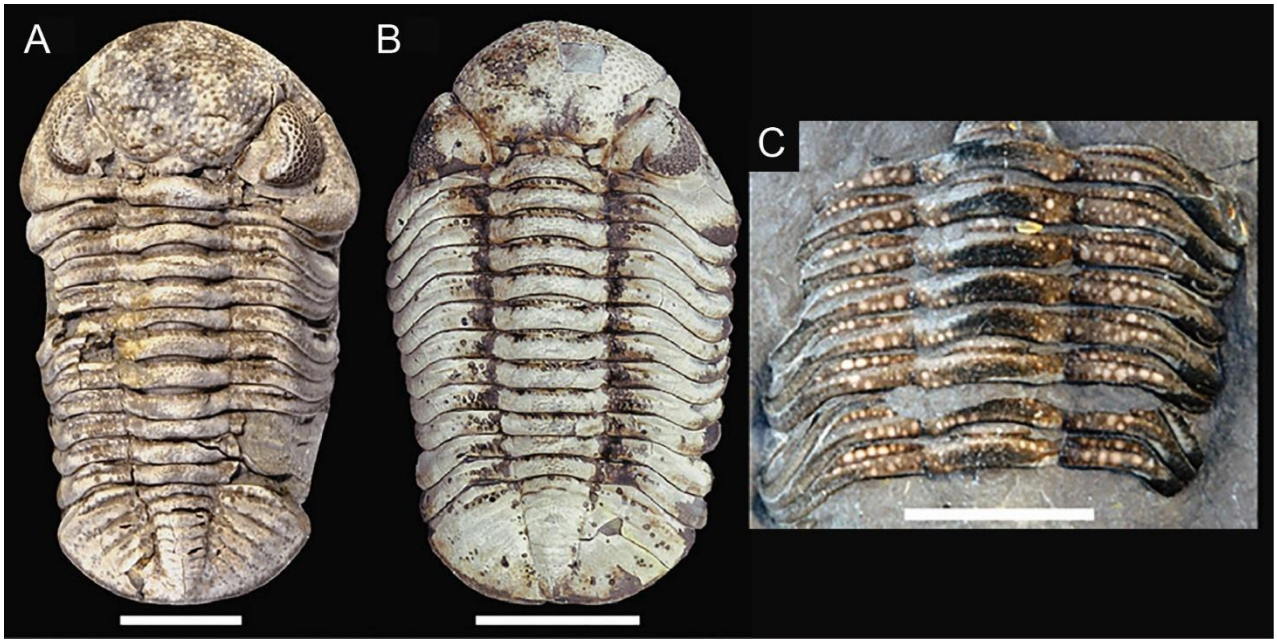

Figure 21. Representative patterns of spotted *E. rana.* A. B. Dorsal view of light-colored exoskeleton with dark-colored spots. C. Dorsal view of an incomplete thorax. Dark-colored exoskeleton with light-colored spots. Image is modified from McRoberts et al. (2013, figure 2). Scale bar = 1 cm.

3.2 Materials and Sample Preparation

3.2.1 Materials

Eight specimens of spotted Eldredgeops rana trilobites of the Middle Devonian (Givetian) Hamilton Group in central and western New York were provided for this study by Dr. Markus Martin and Thomas Hegna. Five samples had a light-colored exoskeleton with darker spots and three samples had a dark-colored exoskeleton with lighter spots. Two specimens with a light-colored exoskeleton were in an extended state, the rest were in a rolled state. For each analysis two samples were analyzed; one light-colored exoskeleton and one dark-colored exoskeleton.

3.2.2 Sample Preparation

specimens were placed in epoxy resin and cut into three sections from the cephalon to the pygidium for a cross-section view of the spots. Grinding and polishing were done on Buehler abrasive paper and MicroCut discs (ranging from P280 to P2500) in three-minute intervals, and with a 1.0 and 0.3 micron MicroPolish for 10 and 5 minutes, respectively. For SE imaging samples were etched in 2% hydrochloric acid for 20 seconds and then gold coated for 1 minute using a sputter coater. For EDS and EBSD they were polished and coated with a 2.5 nm thick layer of carbon using a Gatan 681 coater. For AFM, the samples were polished and etched in 1% acetic acid for 10 seconds.

3.2.3 Analytical Techniques

All the samples were initially characterized using a Nikon SMZ1000 stereomicroscope. SE imaging was done on JEOL 7000 FE-SEM operated in high vacuum mode, at 20 kV, medium beam current (6-13 μA) and 10 mm WD. EDS analysis was done with the same settings using Oxford Aztec software. The samples were also characterized by EBSD. EBSD maps were acquired

using TESCAN LYRA Focused Ion Beam (FIB) -FE SEM in high vacuum mode, at 25 kV, high beam intensity (beam current of 16-18 µA, 10 mm WD and approximately 0.5 step size. Further analysis of the EBSD maps was done using EDAX OIM software. AFM imaging was performed using a Digital Instruments Dimension 3100 equipped with a Nanoscope IV controller under vacuum in tapping mode. Raman analysis was done using a WITec's alpha 500R confocal Raman microscope.

3.3 Results

Optical microscopy imaging confirmed that the spots of the *E. rana* are embedded in the exoskeleton (Fig. 22B). Their size and location in the exoskeleton vary; some are adjacent to the external or internal surface of the exoskeleton, and some are centered in the exoskeleton. In both the light-colored and dark-colored exoskeletons, the spots are circular-oval, and some present a dark-colored rim. The spots are isolated, closely packed with clear boundaries, or fused with unclear boundaries (Fig. 22D and Fig. 23D). Some spots exhibit lamellar structures, which are also present in the exoskeleton (Fig. 22E).

In the light-colored *E. rana*, the color of the spots is darker than the color of the surrounding exoskeleton. In the dark-colored *E. rana*, the color of the spots is lighter than the color of the surrounding exoskeleton. Pyrite replacement is evident in the interior body of the dark-colored *E. rana*, but not in the exoskeleton (Fig. 23B). Schizochroal eyes are visible in the cross section of the light-colored trilobite (Fig. 22C).

SE imaging of *E. rana* revealed that the spots are composed of well-preserved microcrystals. The spots are fully surrounded by the exoskeleton; they do not have an outlet to the exterior surface of the exoskeleton (Fig.24B-24F). The crystals of the exoskeleton are smaller than the crystals of the spots and exhibit an elongated orientation (Fig. 25D and 25E).

EDS point analysis was done on four spots, and three locations in the *E. rana* exoskeleton. The analysis confirmed McRoberts et al. (2013) findings that the spots and the exoskeleton's chemical composition is nearly identical: both are low-Mg calcite with trace amounts of Sr, Mn, Fe, and Na. The analysis revealed that there are slight differences in the Mg and Mn between the spots and the exoskeleton. The spots have 1.1-1.8 wt% Mg and 0.38-0.56 wt% Mn. The exoskeleton has 0.38-0.56 wt%. Mg and 0.18-0.31 wt%.

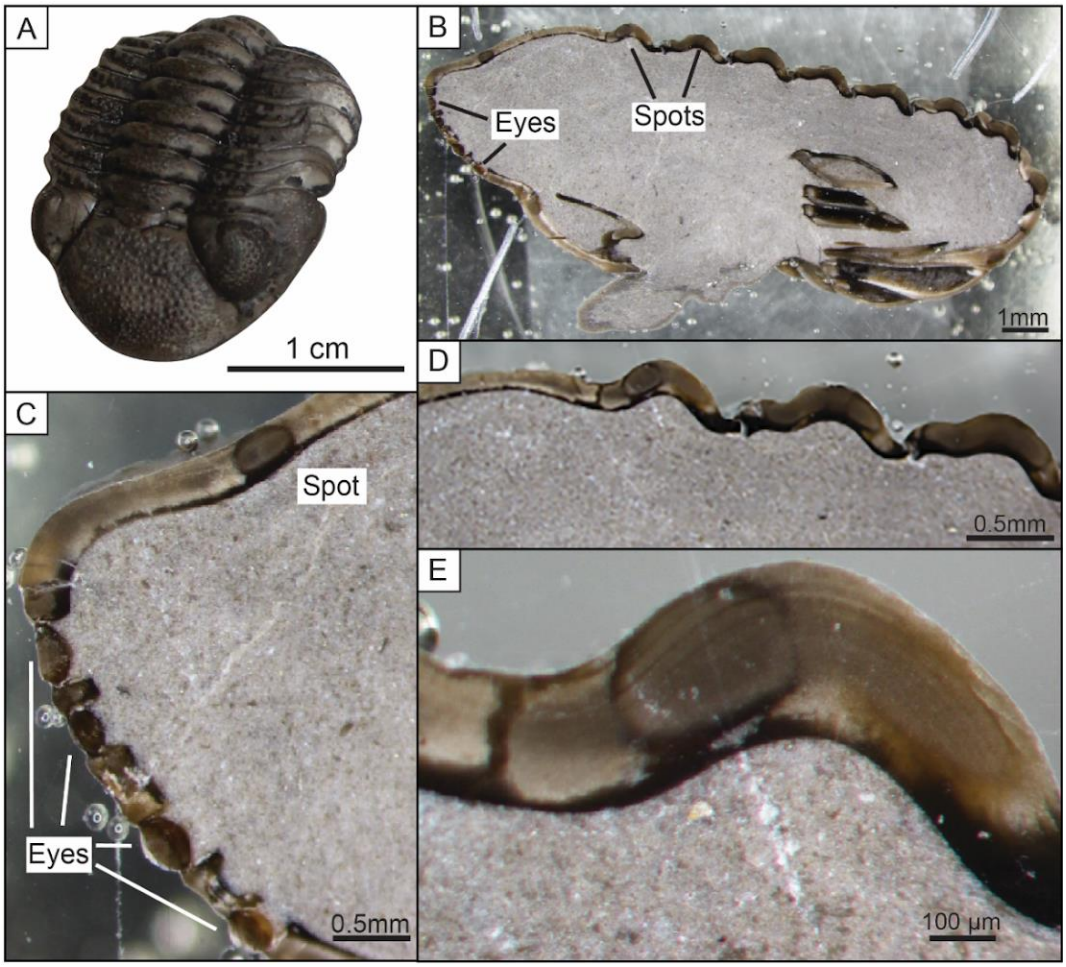

Figure 22. Optical microscope images of a light exoskeleton *E. rana* trilobite. A. An *Eldredgeops rana* trilobite with dark spots. B-E. Cross section images of A, showing the exoskeleton, the dark colored spots, and the eyes (schizochroal). Some of the spots have a dark ring.

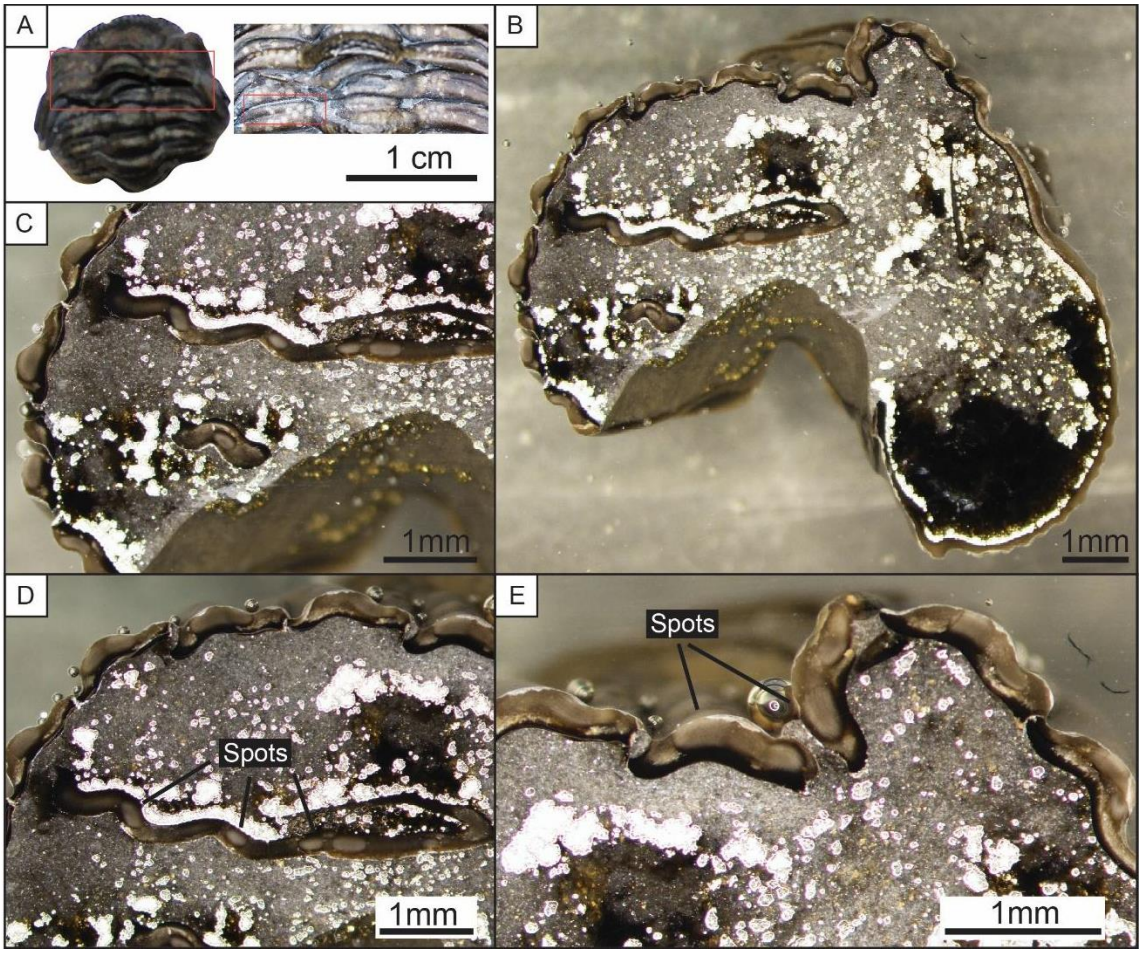

Figure 23. Optical microscope images of a dark exoskeleton *E. rana* trilobite. A. A curled up *Eldredgeops rana* trilobite. Light color spots are seen on the thorax. B-E. Cross section images of A, showing the presence of pyrite and the spots embedded in the exoskelton. All the spots are light in color, and some have a dark ring.

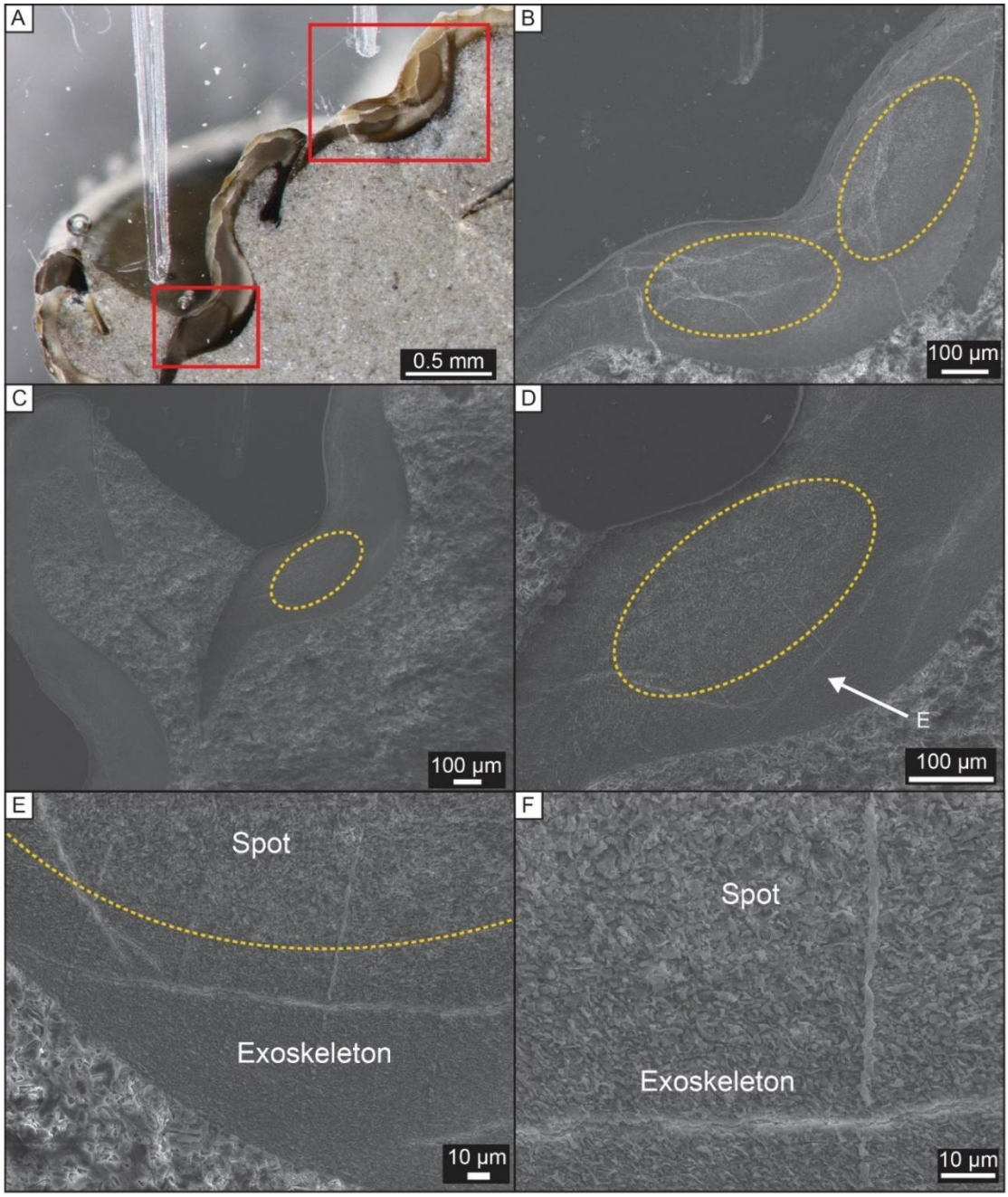

Figure 24. SE images of spots in light colored exoskeleton. A. Optical microscopy image. The red rectangles highlight the areas that have been imaged in SE. B. Two spots highlighted by the yellow dash line. C-D. One spot highlighted by the yellow dash line. E. Show the crystal size difference between the spots and the exoskeleton. The yellow dash line represents an estimation of the spot boundary. F. Higher magnification of E shows the transition of crystal size between the spot and exoskeleton.

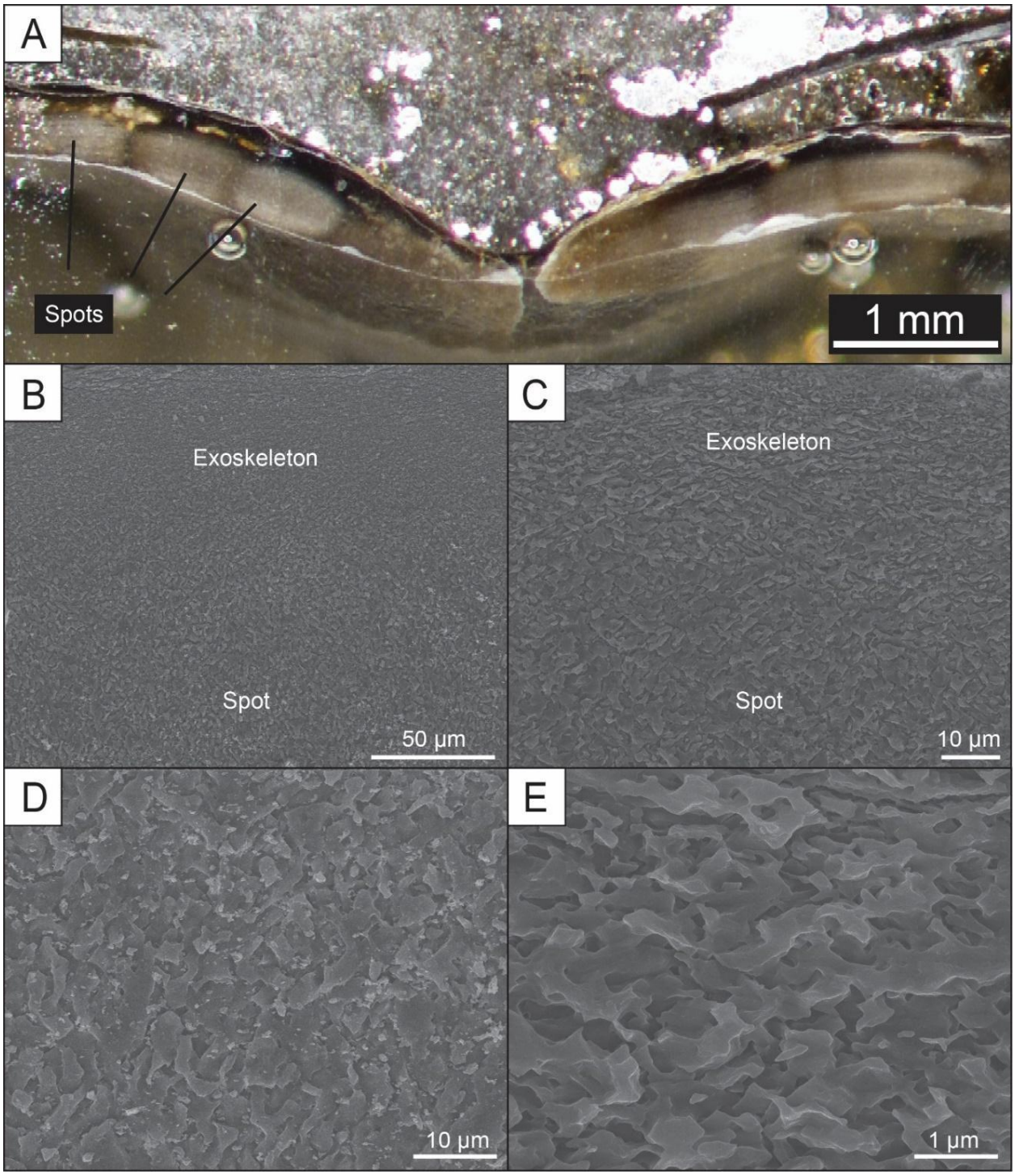

Figure 25. SE images of spots in dark colored exoskeleton. A. Optical microscopy image. Note the pyrite and poor definition of the boundaries of the spots. B-C. SE images show the crystal size difference between the exoskeleton and the spot. Note the compaction of the crystals in the exoskeleton. D. The larger crystals in the spot. E. The smaller crystals in the exoskeleton.

Spots in light exoskeleton	Light exoskeleton	Spots in dark exoskeleton	Dark exoskeleton
1.355	0.905	1.036	0.594
2.162	1.352	1.281	0.487
2.332	1.467	1.841	0.626
2.395	1.695	1.901	0.626
2.531	1.764	1.951	0.752
2.597	1.785	1.989	0.754
2.667	1.803	2.021	0.866
2.892	1.873	2.047	0.875
2.892	1.909	2.110	0.892
2.945	1.937	2.176	0.913
2.945	1.971	2.266	0.988
2.971	1.975	2.352	0.998
3.084	2.153	2.681	1.005
3.394	2.36	4.060	1.008
3.642	2.427	4.100	1.059
3.833	2.457	4.170	1.081
4.037	2.524	4.473	1.087
4.229	2.642	4.67	1.096
4.404	2.952	5.530	1.308
5.027	3.479	6.060	1.506

Table 1. Lengths of crystals in spots and exoskeleton of *E. rana* (in micrometer).

EBSD mapping confirmed the presence of multiple crystals in the spots, with clear crystal boundaries at various orientations (Fig. 25 and 26). Crystal measurements revealed that the crystals in the spots are between 1-6 μm in length (Fig. 27B and Table 1), and the crystals in the exoskeleton are under 3 μm in length (Fig. 27D and Table 1). There is no consistency in c-axis orientation amongst the spots in the light-colored *E. rana*, while there is variation within the spots (Fig. 26C). The c-axis orientation in the dark-colored *E. rana* is identical around the 0°, perpendicular to the surface.

Two-dimensional AFM imaging of *E. rana* show that the crystals in both the exoskeleton and the spots have an angular/sub-angular shape and appear to be similar in size (Fig. 28A and

28C). Three-dimensional AFM imaging reveals that the spots are larger (Fig. 28B and 28D).

Raman spectral analysis identified four variations in chemical composition of *E. rana*: the exoskeleton, the spots, the rim of the spots, and the interior of the trilobite (Fig. 29D). The boundary between the exoskeleton and the interior of the trilobite has the same composition as the rim of the spots. The *E. rana* is characterized by Raman spectroscopy in the range of 200-2200 cm^{-1}. The exoskeleton, the spot, and the rim have two prominent peaks at ~275 and 1150 cm^{-1}. The interior part has four prominent peaks at 800, 1150, 1500, and 1600 cm^{-1} (Fig. 29E).

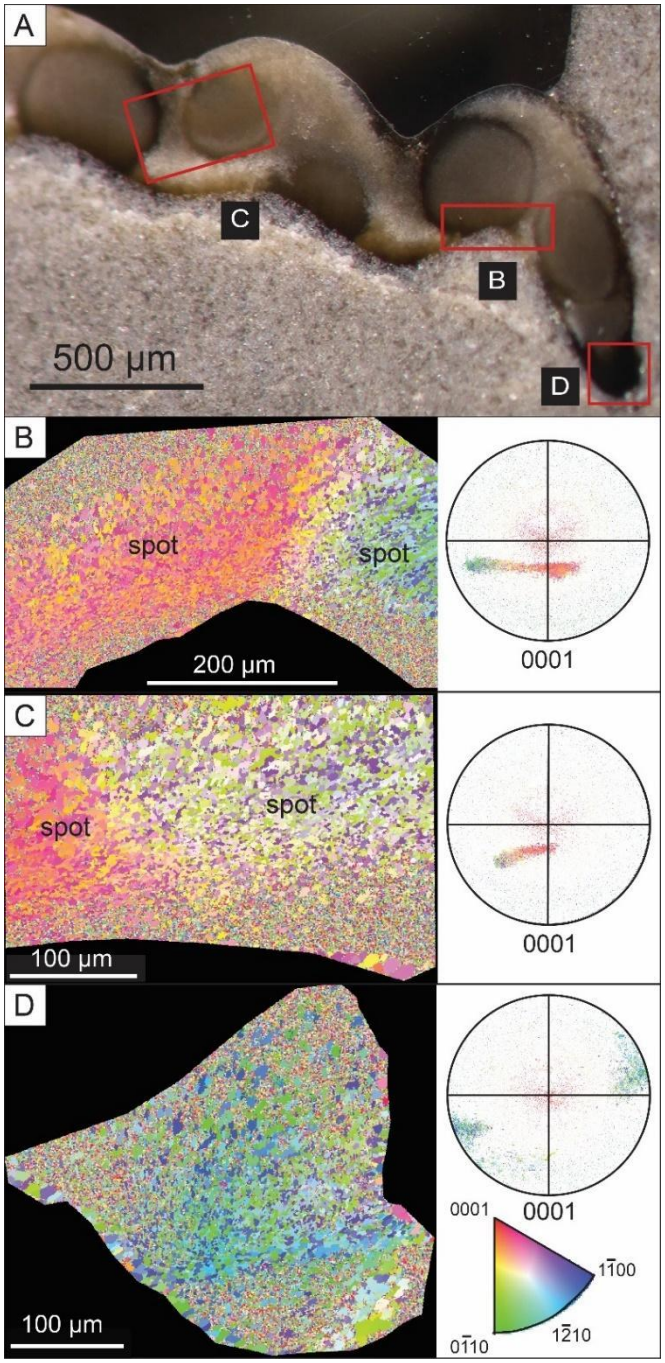

Figure 26. Spots crystal orientation in light colored exoskeleton. A. Optical microscopy image of cross section. Red rectangles correlate to B-D. B-C. Crystallographic maps showing the crystal boundaries and orientation in the spots and their corresponding pole figures. D. A crystallographic map showing the crystal boundaries and orientation in the exoskeleton and its corresponding pole figure. The pole figures show the crystallographic orientation of calcite crystals in reference to the {0001} plane. The colors represent different planes of calcite as shown in the color key in D.

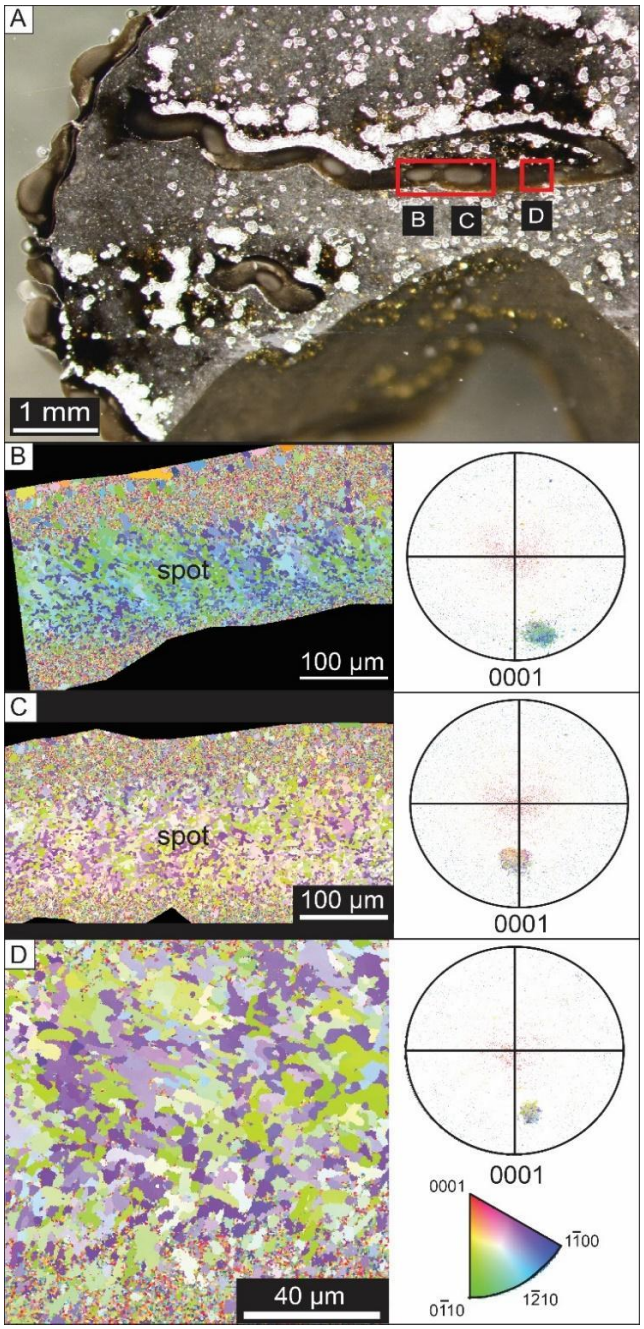

Figure 27. Spots crystal orientation in dark colored exoskeleton. A. Optical microscopy image of cross section. Red rectangles correlate to B-D. B-C. Crystallographic maps showing the crystal boundaries and orientation in the spots and their corresponding pole figures. D. A crystallographic map showing the crystal boundaries and orientation in the exoskeleton and its corresponding pole figure. The pole figures show the crystallographic orientation of calcite crystals in reference to the {0001} plane. The colors represent different planes of calcite as shown in the color key in D.

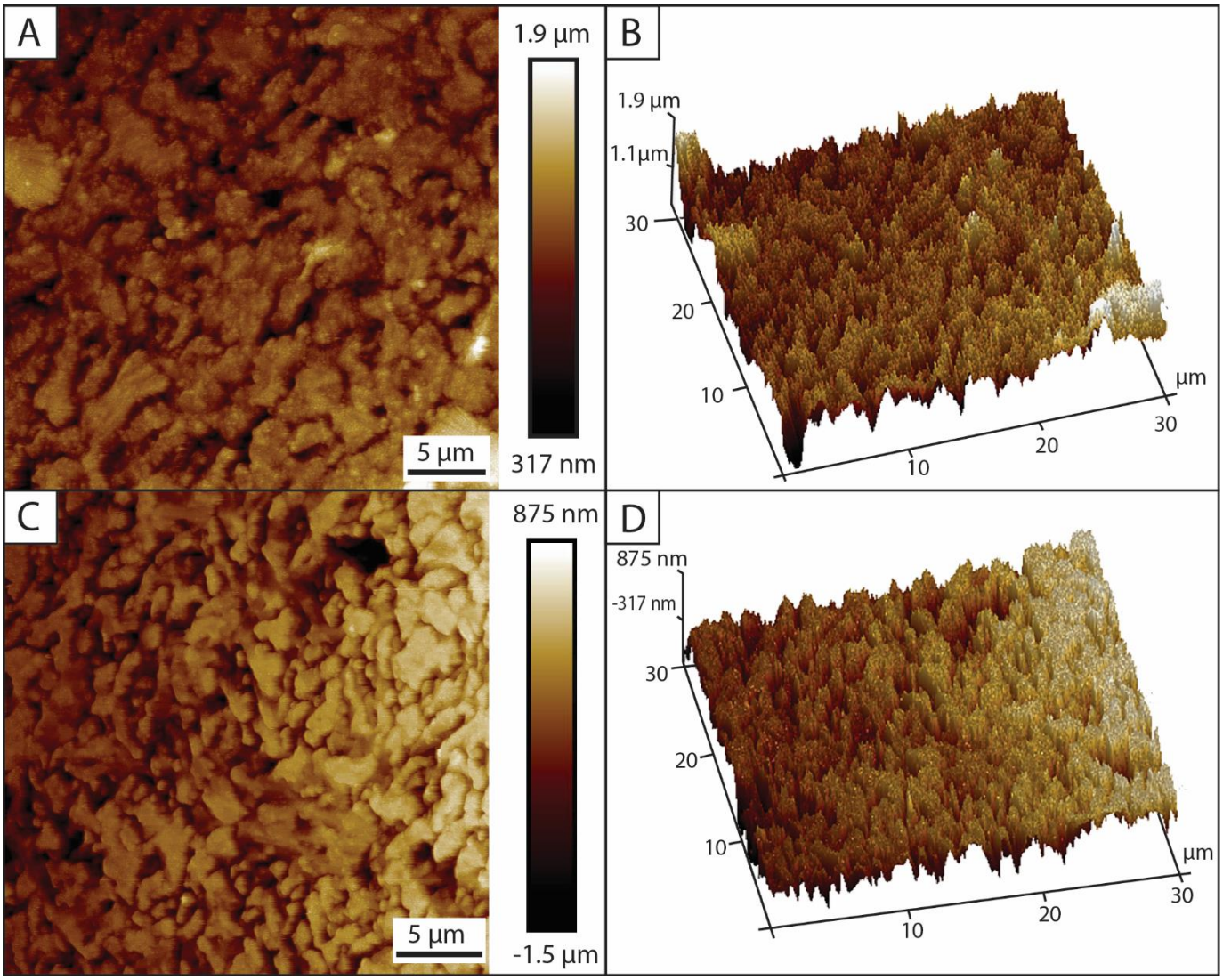

Figure 28. AFM images of spots and exoskeleton in *E. rana*. A. Two-dimensional image of the crystals in a spot. B. Three- dimensional image of the crystals in a spot. C. Two-dimensional image of the crystals in the exoskeleton. D. Three-dimensional image of the crystals in the exoskeleton.

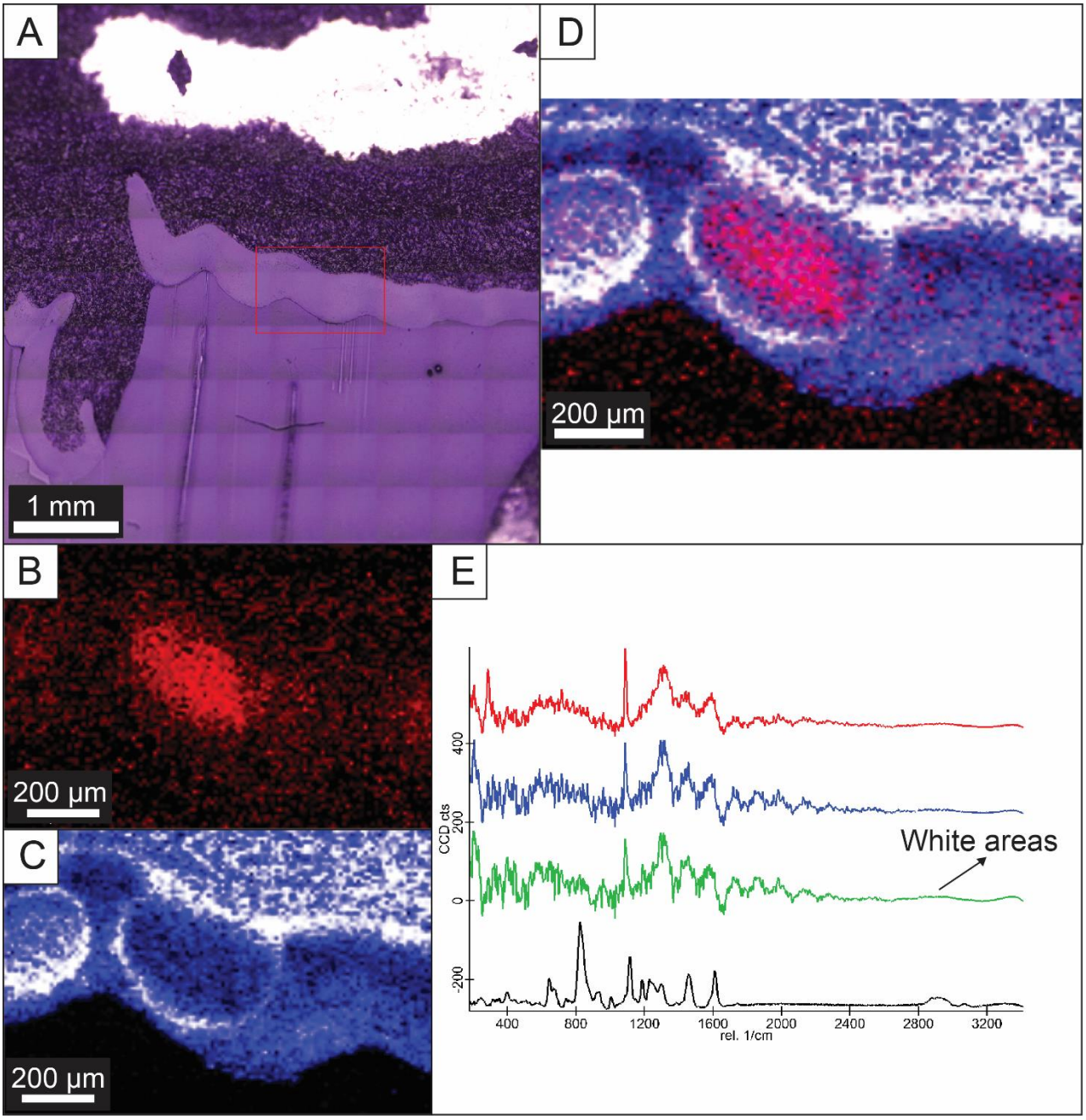

Figure 29. Raman spectrum and spectral images of spots in light colored exoskeleton. A. Image of the exoskeleton. Red rectangle shows the area that has been analyzed. B. Spectral image of a spot. The red area corresponds to the red spectrum in E. C. Spectral image of a spot. The blue and white areas correspond to the blue and green spectrum in E. D. Spectral image of the spots combining the data found in B and C.

3.4 Discussion

3.4.1 Are the spots lenses?

Optical microscopy images show lamellae structure, approximately parallel to the outer exoskeleton surface, similar to growth lamellae seen in schizochroal lenses (Bruton and Haas, 2003). However, coarse lamellae structures, as seen in the spots, can be an indication of recrystallization, and not of growth patterns (Torney, 2010). EDS data confirmed that the spots are low-Mg calcite, contrary to schizochroal lenses of the *E. rana* that are composed of high-Mg calcite. Also, while the core of the *E. rana*'s lenses has a lower concentration of Mg relative to its surrounding features, the spots have a higher Mg concentration relative to the exoskeleton (Torney, 2010).

A visual system would have a pathway connecting the organism's environment to an internal processing system. Optical microscopy images suggested that some spots have an outlet to the exterior of the exoskeleton like the lenses of brittle stars and chitons (Aizenberg et al., 2001; Speiser et al., 2011). SE imaging, however, shows that the crystals adjacent to the external and internal surface of the exoskeleton are different from the crystals of the spots, and are similar to the crystals of the exoskeleton (Fig. 24). This data shows that the spots do not have an external and internal outlet.

EBSD data strengthen this claim, showing that in the region closest to the internal part of the trilobite, the crystals are small relative to the spots, and similar to the exoskeleton (Fig. 26A and 26C). The pole figures reveal that the c-axis orientation of the spots is not consistent amongst the spots, and in some cases is similar to the exoskeleton (Fig.27C, 27D, 26B, 26D). EBSD mapping does not show microstructures that have been previously identified in schizochroal eyes (Torney et al., 2014; Fig. 4).

3.4.2 Are the spots ACC?

Raman analysis performed on a series of Mg-bearing synthetic ACC found that low-Mg ACC has a strong peak at approximately 1080 cm^{-1} (the spectral region carbonates is 1030-1130 cm^{-1}), while high-Mg have a weak peak in the same region (Wang et al., 2011). Raman results show a strong peak at approximately 1150 cm^{-1} (Fig. 29E), consistent with low-Mg composition. Wang et al. (2011) reveal that as the Mg concentration increases, the ACC shape becomes more angular; low-Mg ACC is round. AFM images of the crystal spots and exoskeleton of *E. rana* show that the shape of both is angular and sub-angular, inconsistent with low-Mg ACC. ACC identified in other arthropods, such as crayfish and blue crabs show a sub-round/round shape (Habraken et al., 2014; Dillaman et al., 2005).

3.4.3 Other possible explanations

Shell diseases might be the cause for the spotted appearance of the exoskeleton. Modern day crustaceans suffer from shell diseases resulting in lesions, pits or discoloration of the exoskeleton (Porter et al., 2001). The diseases are caused by a mixture of microorganisms including, fungi, virus and bacteria. Similar sphere-shaped structures have been identified in the clawed lobster *Homarus americanus.* Mineralized granulomas are found in the lobster's antennal glands and cuticular pearl formation is observed in the inflamed areas of the dermis of the lobster (Dove et al., 2004; Smolowitz et al., 1992). Spots on crustaceans' exoskeletons are also caused by the White Spot Syndrome Virus (WSSV). In WSSV-infected shrimp, sphere-shaped inclusions developed in the exoskeletons (Srituyalucksana et al., 2006).

Camouflage or habitat mimicry could both be a possible explanation for the spots. Camouflage is defined by a color pattern of patches or spots resembling the habitat of the animal so that the predator does not identify the prey against the background. Habitat mimicry is defined

as an organism resembling a specific structure in the environment to avoid being identified as prey (Hacker and Madin, 1991). There are numerous examples of arthropods that resemble their habitat and gain protection from predators, including insects, crabs and shrimps (Wickler, 1968; Wicksten, 1983). The patterns displayed by them vary in size, shape, color and brightness.

3.5 Conclusions

Samples of *E. rana* with spots on their exoskeleton were examined to determine if the spots are lenses, serving as a secondary visual system, or ACC spheres serving as a calcite reserve for molting. Optical and electron microscopy shows that the spots cannot be lenses; they are embedded in the exoskeleton, with no outlet to the exterior surface of the exoskeleton. EDS data shows that they are composed of low-Mg calcite, while the lenses of the *E. rana* are composed of high-Mg. EBSD data reveals that the c-axis orientation of the spots is inconsistent. The angular shape of microstructures in the spots indicate that they cannot be low-Mg ACC. The spots may be a remnant of a disease that impacted the *E. rana* in the region or camouflage or habitat mimicry developed by the species as a form of protection from predators.

CONCLUSIONS

The use of high-resolution microscopy and spectroscopy in this study allowed for a greater understanding of rare biomineralization structures in trilobites. In the first case study, SE imaging revealed three types of lenses in the stalked trilobites: a prism, a truncated prism, and a cone. A prism shaped lens has been documented in *Asaphus* sp., but the existence of a cone shaped lens has only been a suggestion in previous studies. The cone shaped lenses are similar to the crystalline cones seen in apposition compound eyes in modern crustaceans and insects. The variation of cone and prism in two of the species could be explained by sexual dimorphism as seen in modern insects. The resemblance to modern arthropods provides evidence for a stronger phylogenetic link between trilobites, crustaceans and insects within the Arthropoda. It also suggests that similar to modern arthropods, the trilobites were able to see low-resolution images. EDS analysis shows that the lenses are low-Mg calcite, indicating they are well preserved despite diagenesis evident by the presence of microdolomite. EBSD data reveals the original structure of the lenses and their optical orientation. It also suggests that the lenses form from lamellar calcite, providing insights to the biomineralization processes that formed the lenses. The discovery of cone shaped lenses shows there is more to learn about the internal structure of trilobite eyes. Further studies of eyes and other preserved structures could provide important information about the trilobite tree and their place in evolution.

In the second case study, light microscopy and EDS analysis confirmed that the spots are embedded in the exoskeleton and that there is no compositional difference between the spots and the exoskeleton. EBSD data indicates that the spots cannot be lenses because they are composed

of microstructures without a uniform, preferred orientation. Raman and AFM analysis reveals that the spots cannot be pockets of ACC because they are low-Mg and are angular and sub-angular. The spots may be a remnant of coloration used for protection or a disease that inflicted the trilobites in that area. Both possibilities suggest a unique occurrence in the environment these trilobites inhabited that has not occurred in other locations where *E. rana* has been found. Overall, the results of these study cases demonstrate that by applying new concepts from the study of modern organisms and using advanced analytical techniques, we enhance our understanding of the diversification of trilobites.

REFERENCES

Addadi, L., Raz, S., Weiner, S. 2003. Taking advantage of disorder: Amorphous calcium carbonate and its roles in biomineralization. *Advanced Materials*, 15: 959–970.

Aizenberg, K., Tkachenko, A., Weiner, S., Addadi, L., Hendler, G. 2001. Calcitic microlenses as part of the photoreceptor system in brittlestars. *Nature*, 412: 819-822.

Albéric, M., Bertinetti, L., Zou, Z.Y., Fratzl, P., Habraken, W., Politi, Y. 2018. The crystallization of amorphous calcium carbonate is kinetically governed by ion impurities and water. *Advanced Science*, 5: 1701000.

Baker, R.H., Wilkinson, G.S. 2001. Phylogenetic analysis of sexual dimorphism and eye-span allometry in stalk-eyed flies (diopsidae*). Evolution*, 55: 1 373–1385.

Bell, M.A., Braddy, S.J. Cope's rule in the Ordovician trilobite family Asaphidae (order Asaphida): patterns across multiple most parsimonious trees. *Historical Biology*, 24(3): 1-8.

Cameron, C.B., Bishop, C.D. 2012. Biomineral ultrastructure, elemental constitution and genomic analysis of biomineralization-related proteins in hemichordates. *Proceeding of The Royal Society*, B.279: 3041–3048.

Clarkson, E. N. K. 1973. The eyes of *Asaphus raniceps* Dalman (Trilobita). *Palaeontology*, 16: 425-444.

Clarkson, E. N. K., Levi-Setti, R., Horváth, G. 2006. The eyes of trilobites: the oldest preserved visual system. *Arthropod Structure and Development*, 35: 247-260.

Cusack, M., Dauphin, Y., Chung, P., P**é**rez-Huerta, A., Cuif, J.P. 2008. Multiscale structure of calcite fibers of the shell of the brachiopod *Terebratulina retusa*. *Journal of Structural Biology*, 164: 96-100.

Dalingwater, J.E. 1973. Trilobite cuticle microstructure and composition. *Palaeontology*, 16: 827-839.

Dillaman, R., Hequembourg, S., Gay, M. 2005. Early pattern of calcification in the dorsal carapace of the blue crab, *Callinectes sapidus*. *Journal of Morphology*, 263: 356-374.

Dove, A.D.M., LoBue, C.P., Bowser P.R., Powell, M.D. 2004. Excretory calcinosis: a new fatal disease of wild American lobsters, *Homarus americanus*. *Diseases of Aquatic Organisms*, 58: 215-221.

Engel, J. 2017. Biominerals and their functions in different organisms. *A critical survey of biomineralization: control, mechanisms, functions and material properties*, 59-62.

Evans, J.S. 2019. Composite materials design: Biomineralization proteins and the guided assembly and organization of biomineral nanoparticles. *Materials*, 12: 581.

Feng, Q. 2011. Principles of calcium-based biomineralization. *Progress in molecular and subcellular biology*, 52: 141-197.

Fordyce, D., Cronin, T.W. 1993. Trilobite vision: a comparison of schizochroal and holochroal eyes with the compound eyes of modern arthropods. *Paleobiology*, 19: 288-303.

Fortey, R.A., Wilmot, N.V. 1991. Trilobite cuticle thickness in relation to palaeoenvironment. *Paläontologisch Zeitschrift*, 65: 141–151.

Fortey, R.A., Ownes, R.M. 2003. Feeding habits in trilobites. *Palaeontology*, 42(3): 429-465.

Fox, D.L. 1972. Chromatology of animal skeletons: Wide and diversified color manifestations from either microstructurally induced chromogenesis or the presence of true pigments. *American Scientist*, 60: 436–437.

Fryer, G. 1968. Evolution and adaptive radiation in the Chydoridae (Crustacea: Cladocera): a study in comparative functional morphology and ecology. *Philosophical Transactions of the Royal Society of London*, Series B, 254: 221–385.

Hacker, S.D., Madin, L.P. 1991. Why habitat architecture and color are important to shrimps living in pelagic Saragassum: use of camouflage and plant-part mimicry. *Marine Ecology Progress* Series, 70: 143-155.

Habraken, W.J.E.M, Masic, A., Bertinetti, L., Al-Sawalmih, A., Glazer, L., Bentov, S., Fratzl, P., Sagi, A., Aichmayer, B., Berman, A. 2014. Layered growth of crayfish gastrolith: about the stability of amorphous calcium carbonate and role of additives. *Journal of Structural Biology*, 189: 28-36.

Harrington, H.J. 1959. General description of Trilobita. *Treatise on invertebrate paleontology*, O: 38-117.

Hollingworth, N.T.J., Barker, M.J. 1991. Colour pattern preservation in the fossil record: Taphonomy and diagenetic significance. *The process of fossilization*. Columbia University Press, New York, pp. 105-119.

Hughes, N.C. 2003. Trilobite tagmosis and body patterning from morphological and

developmental perspectives. *Integrative and Comparative Biology*, 43: 185-206.
Kobluk, D.R., Mapes, R.H. 1989. The fossil record, function and possible origins of shell color patterns in Paleozoic marine invertebrates. *Palaios*, 4: 63-85.

Land, M.F., Fernald, R.D. 1992. The evolution of eyes. *Annual review of neuroscience*, 15: 1-29.

Lau, T.F., Gross, E.M., Meyer-Rochow, V.B. 2007. Sexual dimorphism and light/dark adaptation in the compound eyes of male and female Acentria ephemerella (Lepidoptera: Pyraloidea: Crambidae). *European Journal of Entomology*, 104: 459-470.

Lee, M.R., Torney, C., Owen, A.W. 2007. Magnesium-rich intralensar structures in schizochroal trilobite eyes. *Palaeontology*, 50: 1031-1037.

Lee, K., Wagermaier, W., Masic, A., Kommareddy, K.P., Bennet, M., Manjubala, I., Lee, S., Park, S. Cölfen, H., Fratzl, P. 2012. Self-assembly of amorphous calcium carbonate microlens arrays. *Nature Communications*, 3: 275.

Li, L., Connors, M.J., Kolle, M., England, G.T, Speiser, D.I., Aizenberg, J., Ortiz, C. 2015. Multifunctionality of chiton biomineralized armor with an integrated visual system. *Science*, 350: 952-956.

Lowenstam, H.A., Weiner, S. 1989. *On Biomineralization.* Oxford University Press, New York, pp. 17-18.

McAllister, J.E., Brand, U. 1989. Primary and diagenetic microstructures in trilobites. *Lethaia*, 22: 101–111.

McCulloch K.J., Osorio D., Briscoe A.D. 2016. Sexual dimorphism in the compound eye of Heliconius erato: a nymphalid butterfly with at least five spectral classes of photoreceptor. *Journal of Experimental Biology*, 219(5): 2377-2387.

McRoberts, C.A., Hegna, T.A., Burke, J.J., Stice, M.L., Mize, S.K., Martin, M.J. 2013. Original spotted patterns on Middle Devonian phacopid trilobites from western and central New York. *Geology*, 41: 607-610.

Miller, J., Clarkson, E.N.K. 1980. The post-ecdysial development of the cuticle and the eye of the Devonian trilobite *Phaco*ps *rana milleri* Stewart 1927. *Philosophical Transactions of the Royal Society of London*, 288: 461-480.

Peng, S., Yang, X., Hughes, N.C. 2008. The oldest known stalk-eyed trilobite, *Parablackwelderia kobayashi*, 1942 (Damesellinae, Cambrian), and its occurrence in Shandong, China. *Journal of Paleontology*, 82: 842-850.

Pérez-Huerta, A., Dauphin, Y., Cusack, M. 2013. Biogenic Calcite Granules--Are Brachiopods Different? *Micron*, 44: 395-403.

Pérez-Huerta, A., Coronado, I., Hegna, T.A. 2018. Understanding biomineralization in the fossil record. *Earth-Science Reviews*, 179: 95-122.

Plachetzki, D.C., Fong C.R., Oakley, T.H. 2012. Cnidocyte discharge is regulated by light and opsin-mediated phototransduction. *BMC Biology*, 5: 10-17.

Schoenemann, B., Pärnaste, H., Clarkson, E.N.K. 2017. Structure and function of a compound eye, more than half a billion years old. *Proceedings of the National Academy of Sciences of the United States of America*, 114: 13489-133494.

Schoenemann, B. 2018. Evolution of eye reduction and loss in trilobites and some related fossil arthropods. *Emerging Science Journal*, 2(5): 272-286.

Simkiss, K. 1986. The processes of biomineralization in lower plants and animals – an overview. *Biomineralization in lower plants and* animals. Oxford University Press, New York, pp. 19-37.

Smolowitz, R.M., Bullis, R.A, Abt D.A. 1992. Pathologic cuticular changes of winter impoundment shell disease preceding and during intermolt in the American Lobster, *Homarus americanus*. *The Biological Bulletin*, 183(1): 99-112.

Speiser, D., Eernisse, D.J., Johnsen, S. 2011. A chiton uses aragonite lenses to form images. *Current Biology*, 21(8): 665-670.

Sritunyalucksana, K., Wannapapho, W., Lo, C.F., Flegel, T.W., Virol, J. 2006. PmRab7 is a VP28-binding protein involved in white spot syndrome virus infection in shrimp. *Journal of Virology*, 80: 10734-10742.

Torney, C. 2010. Mineral eyes - lessons from the natural world. Unpublished PhD thesis, university of Glasgow.

Torney, C., Lee, M.R., Owen, A.W. 2014. Microstructure and growth of the lenses of schizochroal trilobite eyes. *Palaeontology*, 57: 783-799.

Warren, I., Smith, H. 2007. Stalk-eyed flies (Diopsidae): modelling the evolution and development of an exaggerated sexual trait. *BioEssays*, 29: 300–307.

Wang, D., Hamm, L.M., Bodnar, R.J., Dove, P.M. 2011. Raman spectroscopic characterization of the magnesium content in amorphous calcium carbonate. *Journal of raman spectroscopy*, 43: 543-548.

Weiner, S. 2008. Biomineralization: A structural perspective. *Journal of Structural Biology*, 163: 229-234.

Weiner, S., Dove, P.M. 2003. An overview of biomineralization processes and the problem of the vital effect. *Reviews in Mineralogy and Geochemistry*, 54(1): 1-29.

Whiteley, T.E., Kloc, G.J., Brett, C.E. 2002. *Trilobites of New York: An Illustrated Guide*. Comstock Pub. Associates, Ithaca.

Wickler, W.1968. *Mimicry in plants and animals*. McGraw Hill Book Co., New York.

Wicksten, M.K. 1983. Camouflage in marine invertebrates. *Oceanography and Marine Biology Annual Review*, 21: 177-193.

Wilt, F.H. 1999. Matrix and mineral in the sea urchin larval skeleton. *Journal of Structural Biology*, 126:216-226.

Xi-Guang. Z., Clarkson, E.N.K. 1990. The eyes of Lower Cambrian eodiscid trilobites. *Palaeontology*, 33(4): 911-932.